BRNO UNIVERSITY OF TECHNOLOGY

VYSOKÉ UČENÍ TECHNICKÉ V BRNĚ

FACULTY OF MECHANICAL ENGINEERING

FAKULTA STROJNÍHO INŽENÝRSTVÍ

INSTITUTE OF SOLID MECHANICS, MECHATRONICS AND BIOMECHANICS

ÚSTAV MECHANIKY TĚLES, MECHATRONIKY A BIOMECHANIKY

COMPUTATIONAL ANALYSIS OF THE BALL-ON-THREE-BALLS TEST FOR DETERMINATION OF STRENGTH OF CERAMIC LAMINATES WITH RESIDUAL STRESSES

VÝPOČETNÍ ANALÝZA ČTYŘ-KOULOVÉHO TESTU PRO URČOVÁNÍ PEVNOSTI KERAMICKÝCH LAMINÁTŮ SE ZBYTKOVOU NAPJATOSTÍ

MASTER'S THESIS

DIPLOMOVÁ PRÁCE

AUTHOR — **Bc. JIŘÍ VENSKÝ**

AUTOR PRÁCE

SUPERVISOR — **Ing. OLDŘICH ŠEVEČEK, Ph.D.**

VEDOUCÍ PRÁCE

BRNO 2021

BRNO UNIVERSITY OF TECHNOLOGY
FACULTY OF MECHANICAL ENGINEERING

Assignment Master's Thesis

Institut:	Institute of Solid Mechanics, Mechatronics and Biomechanics
Student:	**Bc. Jiří Venský**
Degree programm:	Applied Sciences in Engineering
Branch:	Engineering Mechanics and Biomechanics
Supervisor:	**Ing. Oldřich Ševeček, Ph.D.**
Academic year:	2020/21

As provided for by the Act No. 111/98 Coll. on higher education institutions and the BUT Study and Examination Regulations, the director of the Institute hereby assigns the following topic of Master's Thesis:

Computational analysis of the ball–on–three–balls test for determination of strength of ceramic laminates with residual stresses

Brief Description:

The B3B (Ball on 3 Balls) test is used to determine the strength of brittle ceramic materials. This method is currently used primarily for monolithic disc–shaped test specimens. However nowadays, materials with layers of different materials containing also (high) levels of residual stresses are becoming more and more common in practice. Presence of residual stresses may then cause a curvature of the whole sample which can complicate the evaluation of strength using the recent B3B test methodology (originally defined for planar samples). For monolithic planar samples, there is a known relationship between the critical loading force and the maximum stress on the sample surface, characterized by a certain factor f, which must be calculated using a numerical FE model (in order to correctly evaluate the test). So far, this coefficient has been derived only for planar monolithic circular disks, therefore the main goal of this work will be to create a computational model that allows to obtain this coefficient also for curved and multilayer samples. This diploma thesis will be solved in cooperation with the University of Leoben, Austria, where the relevant experiments are performed, to which the computational modeling will be related.

Master's Thesis goals:

1) Recherche in the area of experimental methods applicable for determination of strength of monolithic and layered ceramics with a focus on comparison of various methods, showing their advantages, eventually limitations.
2) Create a computational model of a circular/square shape testing samples made of one or several materials with different elastic and thermal characteristics, including also an influence of residual stresses induced by the sintering process.
3) In SW Ansys simulate the ball–on–three balls test on the monolithic material with the aim to compute the "f" factor determining a relation between the loading force and maximal reached stress on the sample.
4) Analyze an influence of the curvature of monolithic circular/square samples on the location of the maximal stress and value of the factor "f". Examine the error upon the strength computation from experiments if the influence of initial curvature of the sample is not taken into account.
5) Define the strength of layered multimaterial testing samples. Analyze an influence of residual stresses on the location of the maximal stress and value of the factor "f". Propose a methodology for determination of strength of the multi–layered samples.

Recommended bibliography:

BÖRGER, A.; SUPANCIC, P.; DANZER, R.. The ball on three balls test for strength testing of brittle discs: stress distribution in the disc. Journal of the European Ceramic Society. 2002, roč. 22, č. 9-10, s. 1425–1436.

DANZER, R.; HARRER,W.; SUPANCIC, P.; LUBE, T.; WANG, Z.; BÖRGER, A.. The ball on three balls test: Strength and failure analysis of different materials. Journal of the European Ceramic Society. 2007, roč. 27, č. 2-3, s. 1481–1485

LUBE, T.; RASCHE, S.; NINDHIA, T. G. T.. A Fracture Toughness Test Using the Ball-on-Three-Balls Test. Journal of the European Ceramic Society. 2015, roč. 36, č. 6, s. 1637–1642.

ANSYS Inc (2019), ANSYS Release 2019R3 User´s Manual, Swanson Analysis Sys. Inc, Pensylvania.

Deadline for submission Master's Thesis is given by the Schedule of the Academic year 2020/21

In Brno,

L. S.

prof. Ing. Jindřich Petruška, CSc.
Director of the Institute

doc. Ing. Jaroslav Katolický, Ph.D.
FME dean

Abstract

This master's thesis deals with numerical simulation of the B3B test. A research in theoretical background was carried out. After that the numerical simulations of the test were performed in many various configurations (flat, curved, curved laminated) for both a disc and a plate. A hyperbolic relation between thickness and f factor was found. Then linear relation between f factor and curvature was found. A possibility of fracture on layer interface was demonstrated. The last part showed how neglecting residual stress in a laminated specimen could lead to incorrect evaluation of experiments.

Keywords

ceramic materials, ball-on-three-balls (B3B) test, FEM, disc, plate, curvature, laminate, residual stress, f factor

Abstrakt

Tato diplomová práce se zabývá numerickou simulací B3B zkoušky. Byla provedena rešerše v souvisejících oblastech. Poté byly provedeny numerické simulace této zkoušky pro mnoho různých konfigurací (rovný, zakřivený a zakřivený vrstvený vzorek) pro disk a desku. Byla zjištěna hyperbolická závislost mezi tloušťkou a f faktorem. Závislost f faktoru na křivosti byla lineární. Byla provedena demonstrace možnosti prasknutí na rozhraní vrstev. Poslední část ukázala, jak by zanedbání vlivu zbytkového napětí mohlo vést ke špatnému vyhodnocování experimentů.

Klíčová slova

keramické materiály, čtyřkoulový test (B3B), MKP, disk, deska, zakřivení, laminát, zbytkové napětí, f faktor

Rozšířený abstrakt

Tato práce se zabývá efektem různých vlivů na vyhodnocení čtyřkoulové (B3B) zkoušky. Práce je rozdělena na dvě hlavní části.

První část práce má rešeršní charakter. V úvodní části jsou popsány unikátní vlastnosti keramik. Keramické materiály nejsou schopny plastické deformace a nevykazují konkrétní hodnoty materiálových vlastností. To je způsobeno vadami v mikrostruktuře, které jsou důsledkem výrobních procesů.

Dále se práce věnuje klasickým mechanickým zkouškám ke zjištění meze pevnosti keramik. Tyto zkoušky se dělí na tahové, tlakové a ohybové. Zmíněny jsou i biaxiální zkoušky.

Hlavním tématem práce je Ball-on-3-balls (B3B) test, který je blíže popsán. Dále jsou uvedeny různé směry výzkumu v oblasti B3B zkoušky. Mezi tyto patří například geometrické předpoklady, které pokud jsou splněny výrazně snižují výpočetní náročnost numerické simulace zkoušky.

Pro tuto zkoušku byla provedena i intenzivní studie chyb, které mohou pocházet například z geometrie vzorku nebo ze špatné konfigurace testu. Odtud vyplývá jedna z největších výhod této zkoušky oproti ostatním biaxiálním testům. Požadavky na přesnost a tolerance chyb jsou pro vzorky v určitých geometrických mezích velmi nízké v porovnání s jinými zkouškami. Použití této zkoušky má efekt na časovou i ekonomickou stránku.

Zmíněny jsou i další možné způsoby využití této zkoušky. Po vytvoření vrubu na spodní straně vzorku lze tento test použít ke stanovení lomové houževnatosti materiálu vzorku. Tato modifikace se nazývá B3B-KIc test a je poměrně nová. I pro tuto variantu testu byla provedena důkladná chybová studie. Bylo zjištěno, že chyba v natočení vrubu má malý vliv na přesnost zjištěné hodnoty lomové houževnatosti, zatímco malá odchylka polohy vrubu od středu vzorku způsobuje mnohem větší chybu.

Druhá část se zabývá numerickými simulacemi zkoušky se zahrnutím různých vlivů (například křivosti zkušebního vzorku). Všechny dílčí vlivy byly zahrnuty na oba typy vzorků (kruhový disk i deska). Jako první byly vytvořeny modely nezakřivených z jednoho materiálu. Byla provedena série výpočtů pro různé hodnoty

tloušťky vzorku. Z každého výpočtu byla zjištěna hodnota prvního hlavního napětí σ_1 a f faktor udávaící vztah mezi zatěžující silou a napětím na spodní straně vzorku. Následně byly hodnoty vykresleny v závislosti na tloušťce a byla nalezena optimální závislost mezi těmito veličinami. Pro tyto veličiny byla zjištěna hyperbolická závislost s velice dobrou přesností proložení dat. Tato závislost platí pro disk i desku.

Dále byl přidán vliv zakřivení vzorku. Byly vytvořeny celkem tři modely, jeden pro disk a dva pro desku. Zakřivení desky může být totiž bráno buď jen v jednom směru a nebo v obou (v praxi se vyskytují obě varianty). Pro všechny modely s jednotlivými tloušťkami byla zjištěna lineární závislost napětí a f faktoru na křivosti vzorku.

Dále byl studován vliv přítomnosti více vrstev různých materiálů po výšce vzorku. Všechny tři zakřivené modely byly rozšířeny o zahrnutí více vrstev z různých materiálů. Uvažované počty vrstev byly 3-5. Na vybraných kombinacích zakřivený vzorek – počet vrstev byla opět ukázána lineární závislost vyšetřovaných veličin na křivosti.

Na modelu vrtveného laminátu byla ukázáno, že k lomu může dojít na rozhraní vrstev namísto spodku vzorku. Tohoto efektu bylo možno docílit díky rozdílné hodnotě pevnosti sousedících vrstev. V takové situaci by mohlo při vyhodnocování testu dojít k chybnému určení hodnoty f faktoru.

V poslední části byl zahrnut vliv zbytkového napětí. Tento vliv byl znázorněn na symetrickém třívrstvém laminátu pro 3 různé varianty tlouštěk dílčích vrstev. Uvažovaný laminát byl vytvořen ze dvou materiálů s různými hodnotami charakteristické pevnosti σ_0 a koeficientu teplotní roztažnosti α. Pro všechny konfigurace bylo možné ukázat, že v místech maximálního mechanického napětí (střed spodní strany vzorku) po zahrnutí zbytkového napětí došlo k poklesu celkového napětí pod hodnotu pevnosti. Ve vnitřní vrstvě mechanické napětí nepřesáhlo hodnotu pevnosti. Po přičtení zbytkového napětí ale hodnota celkového napětí přesáhla hodnotu charakteristické pevnosti. Tohoto jevu bylo dosaženo pro všechny zvolené kombinace tlouštěk vrtev. K lomu vzorku by v takovém případě došlo na rozhraní vrstev. Opomenutí vlivu zbytkového napětí by mohlo mít velký vliv na správné vyhodnocení experimentu a stanovení f faktoru.

Reference

VENSKÝ, Jiří. *Computational analysis of the ball-on-three-balls test for determination of strength of ceramic laminates with residual stresses* [online]. Brno, 2021. Available from: `https://www.vutbr.cz/studenti/zav-prace/detail/132148`. Master's thesis. Brno University of Technology, Faculty of Mechanical Engineering, Institute of Solid Mechanics, Mechatronics and Biomechanics. Supervisor Oldřich Ševeček.

Declaration

Hereby I declare that this master's thesis is a result of my own work under the supervision of Ing. Oldřich Ševeček, Ph.D. All relevant sources used in this thesis are properly cited and included in the list of references.

.....

Jiří Venský

May 21, 2021

Acknowledgement

I would like to thank my supervisor Ing. Oldřich Ševeček, Ph.D. who has supported me and helped me move forwards with my thesis. I appreciate his attitude and willingness to answer my questions as soon as possible. I would also like to thank Ing. Roman Papšík for his input.

I would also like to thank my family, who believed in me in times I thought it was impossible to complete this thesis. Special thanks belong to two of my friends Josef and Daniel and also my sister, each of them know for what.

Contents

1 Introduction

This thesis deals with a relatively new test for determining the ultimate tensile strength σ_{UTS} of ceramic materials (CM). This test is called Ball-on-3-balls test or 3B3 for short. Figure (1) shows the configuration of the specimen, load and supports of the B3B test [1]. Alternative ways of testing material properties of all materials are being proposed to this day. Research centres aim at creating a test with the reproducibility of results in the first, which is achieved for the conventional tests. But new tests are being developed in order to decrease time needed to perform a test and use smaller specimens so that the experiments become less expensive. In this sense, the B3B test is a very promising alternative to other more conventional tests such as 3 and 4 point bending.

The practical part of this thesis is focused on creating models for finite element (FE) calculations for verification of performed experiments. Two geometrical configurations of the specimen are considered. A disc and a plate. These are two shapes of specimen used for experiments. Models created included effects of different thickness of a flat specimen, curvature a multiple layers on the value of f factor. The last effect discussed in this thesis is the effect of residual stresses on a laminated specimen. The idea is to show how neglecting residual stresses could impact the evaluation of the experiment and bring undesirable errors into the value of the f factor.

The practical part of this thesis is aimed at helping the Montanuniversität in Leoben, where the B3B test is commonly used.

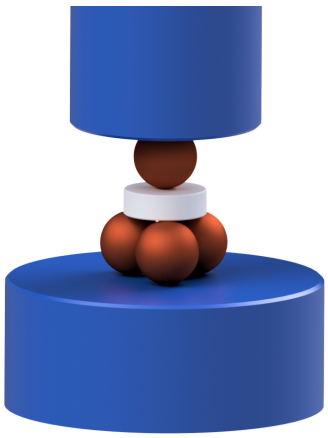

Figure 1: Configuration of specimen and balls in B3B test [1].

2 Analysis of the solved problem

2.1 Problem setting

Determining the ultimate tensile strength σ_{UTS} for ceramic materials had always been a difficult task. The reasons behind this are mainly the stochastic character of material properties of ceramics and their brittleness. Therefore, a number of alternative tests were developed for ceramic materials.

One of those tests is the so called Ball-on-3-balls test (typically shortened as B3B test). Thin specimen (plate or disc shaped) is placed on 3 supporting balls while the fourth ball is used as a punch. After the test is completed, the strength of the material is determined from the fracture force. The constant used for computing the Ultimate tensile strength from the fracture force is called th f factor. Its value is different for every test due to the stochastic character of the properties of ceramic materials. Its value also changes for different geometrical configurations of the test.

The experiment requires a verification via a finite element (FE) calculation.

More recently the problem of evaluating the B3B test for laminates and for specimen with residual stresses has been added to the research of B3B test.

2.2 Problem formulation

FE models for verifying the B3B test for disc and plate specimen with a curvature, laminates and laminates with residual stresses currently do not exist. This work is thus aiming to create such models and perform parametric analyses on them to enable correct evaluation of the ultimate tensile strength also on these types of specimen.

2.3 Aims of the study

- Create the FE models of a disc and plate specimen that is a either a monolithic specimen or a laminate.
- Simulate the test for a monolithic specimen in a FE software. Determine the f factor used to calculate the maximal stress on the specimen.

- Analyze the effect of the curvature of the specimen on the location of the point with maximal value of stress and determine the error in calculation of the maximal stress if the curvature is ignored.
- Determine the ultimate tensile strength of a number of specimen from different materials. Analyze the effect of residual stresses of the location of the point with maximal stress and the value of the f factor.
- Propose a method for creating these models for a laminate specimen with multiple layers.

2.4 System of significant parameters

This section summarizes the previous section into a system of significant parameters [2]. The objects of interest of this thesis are disc and plate specimens used in the B3B test.

S0 (the environment)

The environment of the object is represented by the apparatus of the B3B test and surrounding air. For the means of this thesis all parts of the apparatus are considered to be rigid.

S1 (geometry and topology of the object)

The specimens are thin discs and plates. The models of the specimens are defined by thickness t and either radius r or length of the edge a. Dimensions are considered to be deterministic. One side of specimen is supported by 3 balls and the other is loaded by a 4th ball.

S2 (significant links between the environment and the object)

The supporting balls constrain movement in axial direction of the specimen, so they are considered as simple supports.

S3 (activation of the object)

The specimens are activated by pushing the 4th ball into them.

S4 (interface of processes in the object)

The specimens might be subjected to different effects. These effects are curvature of a specimen, effect of multiple layers and residual stresses. These effects superpose with the load of the specimen and affect its stress state and f factor.

S5 (important properties of the object)

Important properties of the specimens are thickness, material characteristics, characteristic dimension (r or a), parameters describing curvature, thicknesses of layers and coefficients of thermal expansion. First three are essential for f factor analysis of flat specimens. Parameters describing curvature are needed for determining the relation between curvature and f factor. The layers thicknesses are necessary to show how fracture may occur on the interface of two layers. Coefficient of thermal expansion are necessary to include the effect of residual stresses.

S6 (processes and states of the object)

The specimens are subjected to a deformation due the increasing load applied to the pushing ball.

S7 (reaction of the object)

The specimens react to the applied load by a biaxial stress state.

S8 (consequences of reactions)

The consequence of the objects reaction is brittle fracture due to the stress in the specimen reaching a critical value.

2.5 Choice of method of the solved problem

The problem in discussion is direct and is solved through computational modelling. Each of the mentioned effects is simulated for a set of varying geometrical parameters of a model of the specimen. The dependence of f factor on each of the effects will be analyzed.

3 Testing of ceramics

This is the research part of the thesis. Behaviour of ceramic materials is discussed followed by an overview of tests used to determine the strength of ceramics. Brief introduction of Weibull distribution follows. Last part of the research focuses on the B3B test itself and summarizes some of the more recent advancements of the test.

3.1 Unique properties of ceramic materials

Ceramic materials are becoming more common in the technical practice due to their special properties. One of these special properties is the absence of plastic deformation [3]. Ceramics reach its ultimate tensile strength σ_{UTS} right after its yield strength σ_y. There is still a plastic phase in a σ/ϵ diagram but is minimal in comparison to the linear phase. This is the reason why ceramic materials can be modelled as linear all the way until fracture. The main issue is, even though the strength of a ceramic material is measured at a certain value, that the finished product can break under lower load. This happens due to microstuctural inclusions or cracks in its structure [4]. The larger the component is the higher probability of these errors is. This phenomena arises from the production processes such as sintering during which it is almost impossible to create a material with 100 % density meaning there are small bubbles and cracks after the process is finished. This phenomena also occurs with testing specimens.

This is one of the reasons of the implementation of the B3B test. Due to its geometry, the maximum load is in theory only in one point in the middle of the specimen [5]. This fact prevents the interference of errors in the materials structure.

Ceramic materials are commonly used in high temperature environment such as industrial furnaces. This is due to their another useful property, which is heat resistance. This means that ceramics do not subject to creep as much as metal materials [3]. The downside to its applications in high temperature environment is low resistance to thermal shock. This means that, when subjected to rapid temperature changes, cracks might initiate in ceramic materials.

3.2 Tests for determining properties of ceramic materials - Ultimate tensile strength

As was mentioned in previous section 3.1 ceramic materials posses unique properties, which impact the way of tests for determining their material properties. This means that for these materials various tests including common tests with standardizes dimensions are used. This section covers some of these tests.

3.2.1 Tensile test

For fragile materials the ultimate tensile strength σ_{UTS} is the most important property because of the absence of the Yield strength (σ_y). The most common test for determining this value for metal materials is the tensile test [6]. This test is also used for ceramic materials but is not as common. This is due to the fact that if the specimen does not have precise dimensions or the grips are not in one axis, there is a possibility of the specimen breaking in the grips even long before reaching the real material strength. When the tensile test is executed, the strength of the material is calculated from the Force/displacement graph. The formula below in equation (1) is used to calculate the strength of CM from the experiment.

$$\sigma_{UTS} = \frac{F_{max}}{S} \tag{1}$$

Where F_{max} is the maximal force from the experiment and S is the area of the cross section of the specimen. If the requirements are met, the value of the strength is determined by the largest crack in the direction perpendicular to the load [3].

3.2.2 Bending tests

Due to the high demands on precision for the tensile test ceramic materials are tested by bending tests [7]. Those come in two variants.

- Three point bending test
- Four point bending test

The design of these tests as well as course of internal forces are shown in figures (2) and (3). In the case of the 3 point bending test, there exists a shear force near

the point of maximal bending moment, which can theoretically affect the calculated value of the bending strength. On the other hand in the four point bending test the specimen is subjected to pure bending moment.

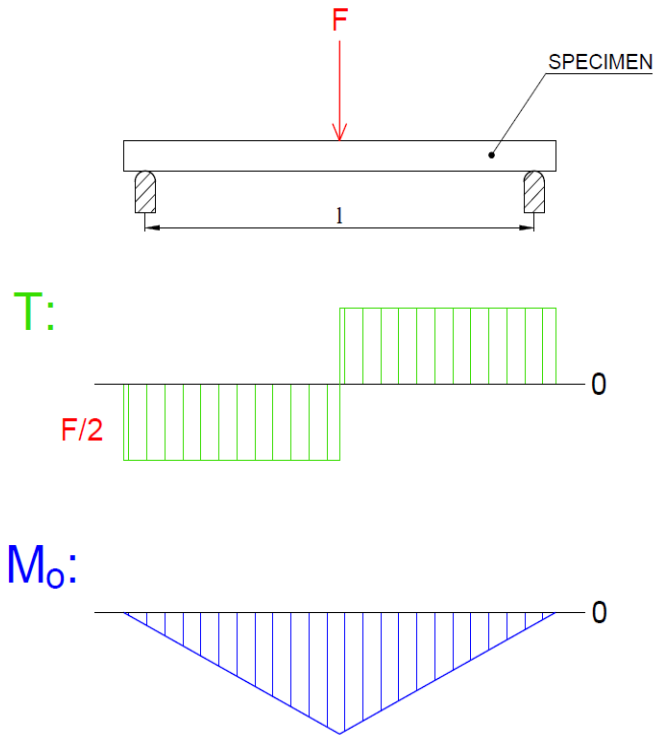

Figure 2: Three point bending test.

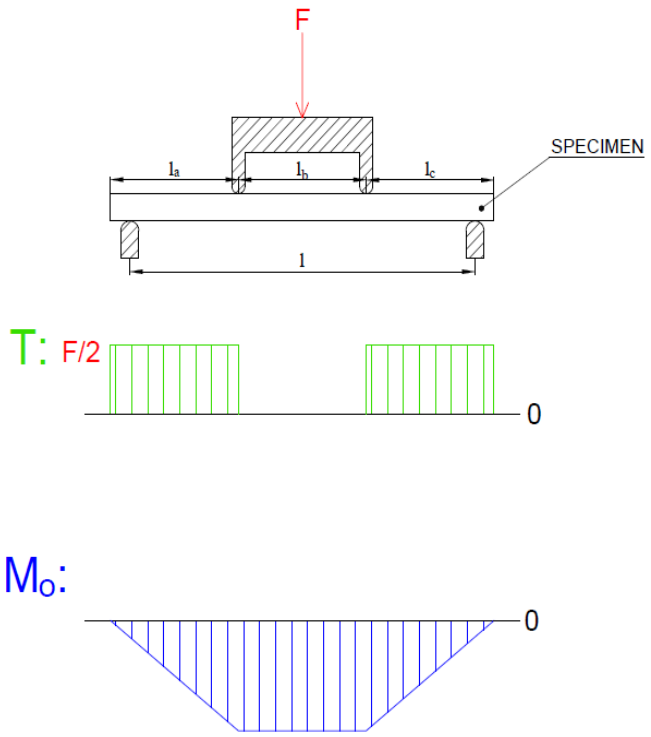

Figure 3: Four point bending test.

In case of the pure bending, the stress in a cross section is distributed linearly with no stress in the middle of the cross-section. This area is called neutral surface [6]. The way the stress is distributed in a cross section during both 3 and 4 point bending test in the middle of the specimen is shown in figure (4).

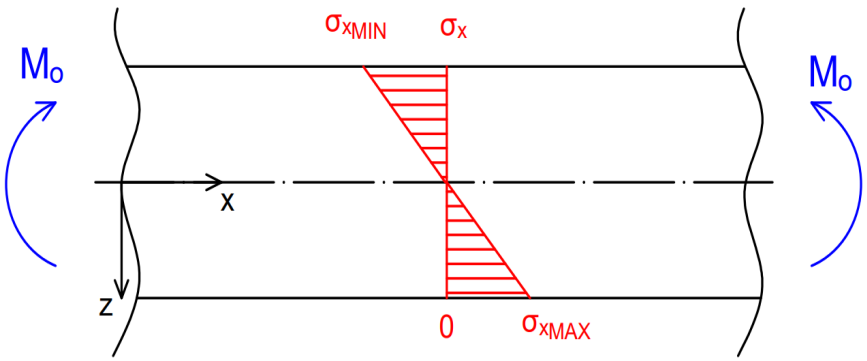

Figure 4: Stress distribution in a cross section of a beam subjected to bending.

In equation (2) the formula to determine the maximal stress σ_{max} for rectangular cross section is stated. In equation (3) appears the formula for circular cross section.

$$\sigma_{max} = \frac{3}{2}\frac{F_{max}l}{bh^2} \tag{2}$$

$$\sigma_{max} = \frac{8}{\pi} \frac{F_{max} l}{d^3} \tag{3}$$

The formulas for both variants of the four point bending test (rectangular and circular cross section) are shown in equations (4) and (5).

$$\sigma_{max} = \frac{3 F_{max} a}{b h^2} \tag{4}$$

$$\sigma_{max} = \frac{16}{\pi} \frac{F_{max} a_{4P}}{d^3} \tag{5}$$

The parameters that appear in equations above are listed below:

- F_{max} – maximal force measured during the test,
- l – distance between both supports in the 3 point bending test,
- a_{4P} – distance from support to the load in four point bending test,
- b and h – dimension of the rectangular cross section specimen (width and height respectively),
- d – diameter of the cylindrical specimen.

These tests are also used for determining the Young's modulus of variety of materials, mainly those with low drawing ductility [7].

Bending tests are also common for composites, because their behavior changes dramatically depending on the character of the loading. This means that most of laminate composites have to be tested with tensile test as well as bending test. For those materials, the four point bending test is far more stable for determining the ultimate tensile strength [8].

3.2.3 Compression tests

The strength of ceramics varies depending on the nature of the load. More often than not their strength in compression is higher than in tension. This can also be observed in bending tests, where the specimen breaks on the other side of the load (the side subjected to tension).

Compression tests are uniaxial. The strength of the material in compression σ_{Rd} is calculated the same way as from the tensile test. The formula is written in equation (6).

$$\sigma_{Rd} = \frac{F_{max}}{S} \tag{6}$$

In the equation F_{max} represents the force at which the fracture occurs while S is the area of the cross section of the specimen.

The high values of compression strength of ceramics create some problems in compression tests [5]. The main ones is clamping of the specimen and a suitable shape. If the specimen is not correctly placed while testing an unexpected tensile stresses might occur leading to improper evaluation of materials strength in compression. The value of the strength is often undervalued.

3.2.4 Alternative tests

This section describes some of the biaxial tests of CM. Those can be divided in two parts [9].

1. Axis-symmetric stress distribution

2. Non axis-symmetric stress distribution

A main disadvantage of most of these tests (ring on ring, ball on ring, ball on ring of balls) is their dependence on the precision of the specimen preparation. Often the polishing treatment is required which increases the costs of the test. An example of non axis-symmetric test is the B3B test closely discussed later.

Ring on ring test

Ring on ring test is an example of axis-symmetric biaxial test. As its name suggests the configuration of this test consists of two rings of different radii [10]. The test is depicted in figure (5) [11]. The specimen is disc shaped. The specimen is placed on on the ring with higher diameter. The specimen is then loaded by the second ring. This creates a linear load on the radius of the smaller ring. Applied force is recorded and its fracture value is then used to calculate the fracture stress via formulas provided in the norm ISO 17167 [10].

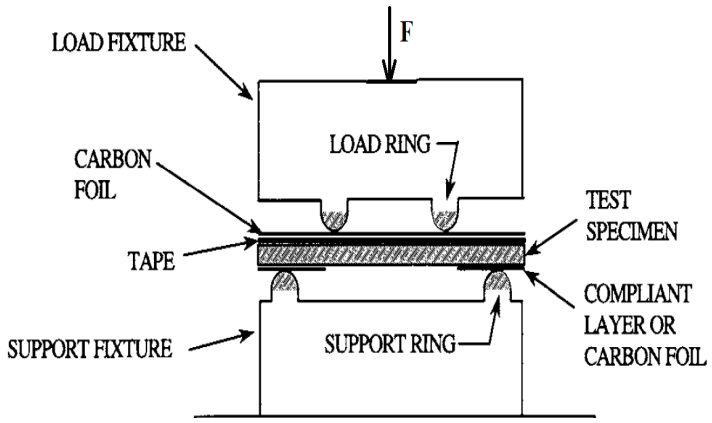

Figure 5: Geometrical configuration of the ring on ring test [11].

3.3 Evaluation of ceramic materials tests

Due to the uncertainty of ceramic tests it is necessary to carry out significant number of tests. Mechanical properties of ceramics are not deterministic values, they are stochastic [12]. The value of any numerical property is then given not by a number but by an interval which respects a certain statistical distribution. In technical practice the distribution of these properties follow 'Weibull's distribution'.

3.3.1 Weibull's distribution

This distribution is dependant on three parameters [13]. The function of the cumulative probability of this distribution is shown in equation (7).

$$F(x) = 1 - e^{-\left(\frac{x-x_0}{a}\right)^b} \tag{7}$$

The three independent parameters are listed bellow:

- x_0 - represents the threshold value of x,
- a - represents the scale of the distribution,
- b - declares the shape of the distribution.

Bellow in figures (6) and (7) the functions that represents Weibull's distribution [13] are shown. These figures were created for the parametric values of $x_0 = 0$, $a = 0,35$ and $b = 1,8$.

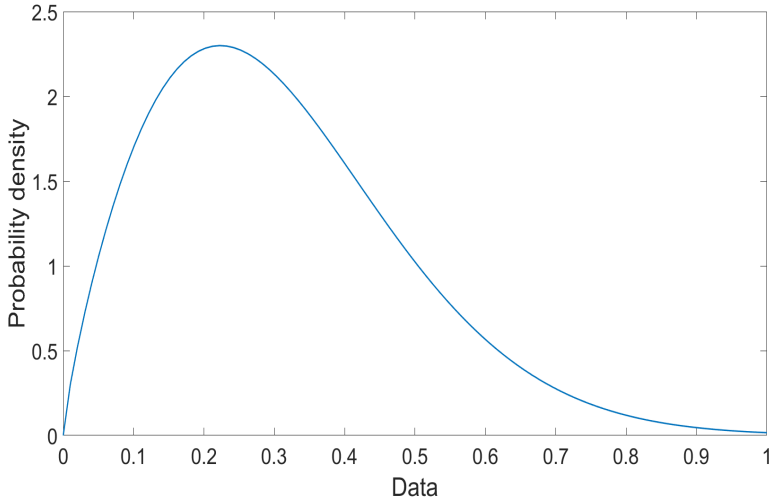

Figure 6: The probability density of Weibull's distribution for parameter $b = 1, 8$ [13].

..

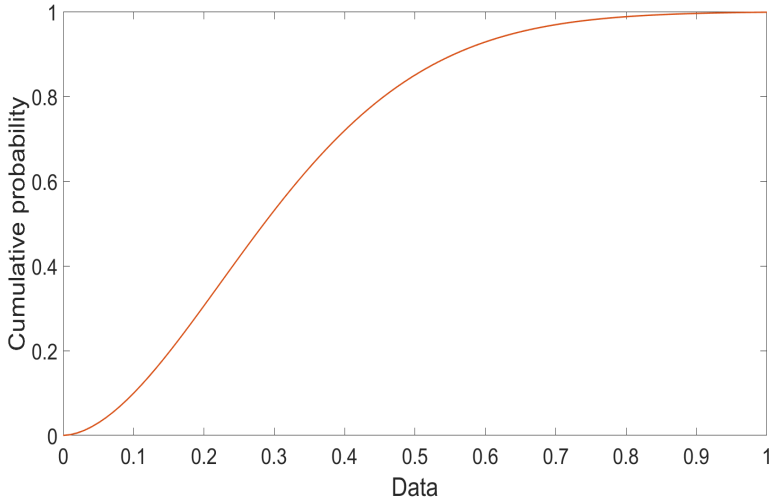

Figure 7: The cumulative probability of Weibull's distribution for parameter $b = 1, 8$ [13].

Weibull'S distribution is flexible in a sense that its shape can dramatically change depending on the value of parameter b [14]. For example, if the value of b is set to 1, Weibull's distribution becomes exponential distribution.

3.3.2 Applying Weibull distribution to material properties

Properties of Weibull's distribution make it one of the most applied distributions for evaluating many stochastic effects in engineering. It is commonly used for example to evaluate time to failure or for evaluating the strength of brittle materials.

Weibull modulus m is a dimensionless parameter which may serve as a material characteristic [14]. In previous segment about Weibull distribution in general its parameters were explained. Weibull modulus represents the parameter affecting the shape of the distribution. When its value rises the distribution becomes thinner. This means that with higher values of Weibull modulus different specimens of the same material reach failure at values closer to each other. The threshold parameter in case of strength of the materials represents the value of stress that every specimen withholds.

3.4 B3B test

In this section the B3B test is described. The 3B3 test is a test with configuration shown in figure (1). This test presents a geometrical composition where one ball is pushed into the specimen which is supported by 3 balls of the same size on the other side. The supporting balls touch each other. Their radius is tied to the radius at which they support the specimen. This connection is written in equation (8) [9].

$$R_a = \frac{2\sqrt{3}}{3} R_b \tag{8}$$

In this equation R_a represents the support radius and R_b the radius of the balls. Figure (8) shows the configuration from above [1].

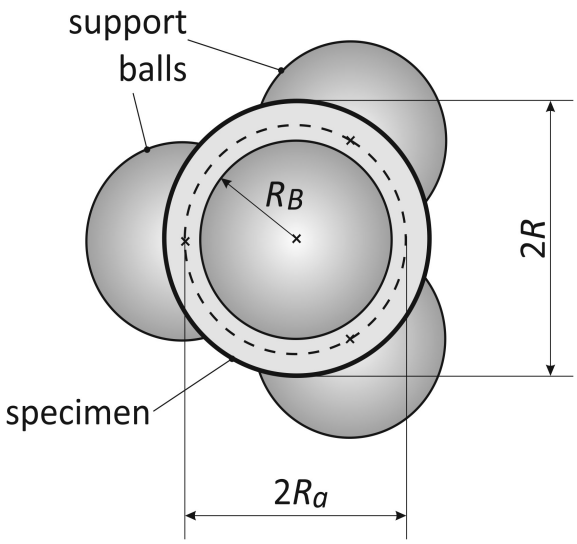

Figure 8: Above look at the B3B configuration [1].

The applied force is measured until the specimen fractures. The most common type of the specimen is a thin disc. Plate shaped specimens could also be used.

The advantage that B3B test possesses over other bi-axial strength tests is in its resistance to geometrical inaccuracies [9]. The fact that the maximum tensile stress is achieved in the middle and not by the edge of the specimen, where manufacturing defects appear, is the reason for the tests tolerance on geometrical inaccuracies.

The stress field in the disc specimen is shown in figure (9) [15]. It has a characteristic cloverleaf shape [9].

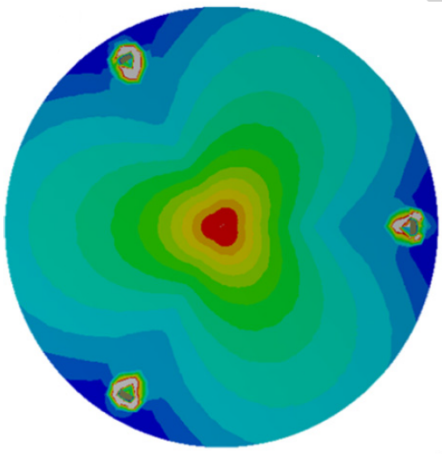

Figure 9: Stress field in standard B3B test [1].

After the initial introduction of this test further research was carried out. The following pages summarize some of the main new concepts and possible potential

improvements in B3B test.

3.4.1 Numerical simulation of the B3B test

This part describes the main focus of a paper by Börger et. al [9]. An analytical approach to the test is also proposed. Main problem is that the analytical approach does not meet the results of both the numerical simulation or the carried-out experiments.

The numerical simulation has been done with rigid bodies representing the disc and both the support balls and the loading ball.

The maximal stress σ_{max} was calculated numerically and these data were inserted into the equation (9). To relate a force to the stress, a dimensionless parameter f is proposed - Eq. (9). This factor depends on both geometry and material.

$$\sigma_{max} = f\frac{F}{t^2} \tag{9}$$

The simulations were carried out for different combinations of Young's moduli and Poisson's ratio ν in order to determine how these parameters affect the shape and size of the contact areas as well as how the parameter f changes.

In conclusion the different variations of the Poisson's ratio had little effect on the contact zones and parameter f. Different variations of Young's moduli (from 100 to 400 GPa for disc and balls) led to bigger differences in both the shape and size of the affected area, but not by much [9]. Therefore it was concluded, that the f factor does not depend on neither elastic moduli and Poisson's ratio of the supporting balls and the Young's modulus of the disc.

It was discovered, that it is not necessary to model this test with complicated nonlinear loading areas [9]. It is suggested that modelling with one point loads is sufficient. It is impossible to ignore area loads for discs of very high or small thickness. This paper proposed that using point loads a is valid approach for these ratios:

$$0,05 < t/R < 0,6 \tag{10}$$

If this ratio is in defined range, the parameter f is also independent of the magnitude of the applied force F.

The most important takeaway is that the maximum tensile stress is always located in the center of the bottom side of the model and its value is proportional to applied force F which can be used instead of modelling contact surfaces [9].

3.4.2 Sources of errors in B3B testing

The main topic of another article by Börger et. al [16] were the sources responsible for possible errors in B3B testing (e.g. friction-less areas of contact).

The dimensionless parameter f is finalized as a function dependent on three ratios [16]. These are R_a/R, where R_a and R are the radius of the supporting balls and the radius of the disc respectively, t/R, where t is the disc's thickness and ν is Poisson's ratio. The finalized function is stated in equation (11) [16].

$$f\left(\frac{t}{R}, \frac{R_a}{R}, \nu\right) = c_0 + \frac{\left(c_1 + c_2\frac{t}{R} + c_3\left(\frac{t}{R}\right)^2 + c_4\left(\frac{t}{R}\right)^3\right)}{1 + c_5\frac{t}{R}}\left(1 + c_6\frac{R_a}{R}\right) \qquad (11)$$

In this equation the terms dependent on Poisson's ratio are the constants c_0 to c_6. In the article, the values of c_i were calculated for 4 different values of Poisson's ratio ranging equidistantly from $0,2 - 0,35$.

In further sections of the article different possible sources of inconsistencies were discussed. First of the sources is the importance of the friction and its relation to the degrees of freedom of the supporting balls [16]. If the supporting balls are fixed, the effect of the friction has to be included. When considering free rolling of the supporting balls, the effect of the friction can be neglected.

Other discussed effects included inclination of the disc and convex disc geometry. Errors in calculations of the maximum tensile stress do not exceed 1 % if the difference between minimum and maximum thickness is smaller than 16 % for standard geometry [16]. The effect of convex geometry can be excluded if the difference in thickness of the specimen in its centre and at its edge is smaller than ±5 %.

The last mentioned effects are the geometrical imperfections. These are all possible excentric positionings of loading ball, disc and one or more supporting balls. It was shown that even though the symmetry of the stress field is disturbed, the value of maximal tensile strength changes minimally.

All of the mentioned effects apply only if the dimensions of the specimen are within certain limits [16]. For extremely thin specimens other fracture modes occur.

On the other hand for extremely thick specimens the failure of the specimen occurs as a result of Hertzian cracks staring inside of the material.

3.4.3 Comparison of the 3B3 test to uniaxial bending tests

A comparison of the B3B test to uniaxial bending tests was the main topic of an article from 2007 by Danzer et. al. [17]. In the first part of the paper the advantages of the B3B test such as low friction and tolerance to dimension error are mentioned [16]. These advantages incited Danzer et. al. to carry out experiments on multiple ceramic materials (alumina and zinc oxides and silicon nitride) in order to compare B3B test with standard bending tests [17].

In the next part the setup is introduced and the article talks about dimensionless parameter f mentioned in the equation (9). The parameter is dependent on three ratios mentioned in equation (11). In this article the ratios have been assigned a symbol. In order they represent the ratio of thickness and disc radius, support radius and disc radius and Poisson's ratio [17]. These ratios are listed below.

- $t/R = \alpha$, $0,05 \leq \alpha \leq 0,60$
- $R_a/R = \beta$, $0,55 \leq \beta \leq 0,90$
- ν, $0,20 \leq \nu \leq 0,30$

In addition, if these ratios find themselves in the ranges above, an analytical approximation exists [17]. The value of the parameter then also roughly lies in range between 1 and 3.

If the specimens are not in these ranges, model for numerical simulation has to be performed to determine the maximal tensile stress [9].

The testing was performed on three different materials as was already mentioned. The silicon nitride ceramic was used for in total 157 tests with 8 various dimensions [17]. The alumina ceramic (aluminium oxide) was used for 315 tests. 14 types of specimens were used in total. The last material (zinc oxide) was used to carry out 166 test with 6 specimen variations.

With higher number of tests the team was able to determine the Weibull parameters (characteristic strength and Weibull modulus) of each set of tests (number

of different specimens) and the 90 % confidence interval of these parameters. These intervals get smaller with higher number of performed tests [17].

The next step lies in comparing the B3B tests stress, which is biaxial, to the stress from bending tests. For these purposes the so-called principle of independent action (PIA) equivalent stress was used [17]. The formula of the PIA equivalent stress is written in equation (12).

$$\sigma_{eq,PIA} = (\sigma_I^m + \sigma_{II}^m + \sigma_{III}^m)^{1/m} \tag{12}$$

In the last part of the paper the results were discussed. Relations between the strength of the material and specimens effective volumes and areas were found. For all materials it was observed that the smaller the specimen the higher the PIA strength was [17].

3.4.4 Application of the B3B test to determine fracture toughness

An article by Strobl et. al. [15] from 2014 dives deeper into the potential of B3B test and tries to use it as a mean to determine the fracture toughness K_{Ic} of a specimen. In the past there were already attempts for measuring K_{Ic} of a small disc specimen such as Small punch test (SPT) [18]. But SPT focuses on metal specimens and those attempts lead to the conclusion that SPT is not very accurate and methods that use specimens with higher dimension are recommended.

In this modification of B3B test (called BRB-KIc test) a crack on the side of the support balls is made [15]. A Knoob indenter is used to create the crack. After its usage an area with residual stress is created. This area needs to be removed (e.g. using a grinder). The thickness of the removed area is determined based on the Surface Crack in Flexure atandard.

Since the nature of the stress field during B3B, it is impossible to achieve symmetrical load of the crack [15]. It is advised to point the tip of the crack towards one of the supporting balls. The proposed formula for calculating the fracture toughness K_{Ic} is shown in equation (13).

$$K_{Ic} = \sigma_{B3B} Y \sqrt{a_{KI}\pi} \tag{13}$$

The parameters in the equation represent in order the stress in the middle of the

bottom side σ_{B3B}, the geometric factor Y (dependent on geometry of the specimen, the crack and Poisson's ratio), and the depth of the crack a_{KI} [15].

Further discussion on the properties of the geometric factor Y follows including some limitations.

Experiments were carried out on specimens from 5 different ceramic materials [15]. All materials were subjected to conventional tests for fracture toughness K_{Ic} as well. Preparations of the specimens was performed. For all used configurations at least 4 tests were performed. One of the disadvantages of this test is the precision it requires for the position of the crack. Even if perfect positioning of the crack is achieved this method gives roughly 3 % higher value of fracture toughness K_{Ic}. On the other side the inclination of the crack (its angle in relation to one of the ball) has little to no effect on the evaluated value of K_{Ic}.

In conclusion, if the crack is correctly positioned even with inclination error, the results match very well with standardised test [15]. Furthermore, its results on very small specimens (diameter down to 5 mm) seem to maintain below 5 % error. Even for this test, the main advantage of the original 3B3 test applies. It is simple and economically viable.

3.4.5 Numerical simulation of the B3B-KIc

Numerical simulations of the B4B-KIc test were discussed in an article by Lube et. al. from 2015 [19]. Meanwhile, the previous articles main focus was to show the validity of the 3B3-KIc test in relation to the traditional test of fracture toughness, this article focuses on accessing this test to engineers outside of the research laboratories. This is achieved by creating an empirical formula for the geometric factor Y. Reordering terms in equation (13) leads to a formula to calculate Y. Substituting for σ_{B3B} the terms in equation (9), the form from which the empirical formula is created can be written - Eq (14).

$$Y = \frac{K_{I,FEM} t^2}{F f \sqrt{\pi a}} \tag{14}$$

The term $K_{I,FEM}$ represent stress intensity factor obtained from finite element calculations.

In the next part the article describes how the FE calculations were performed.

Three different types of deviation of the crack were evaluated [19]. These are translational deviations from the center in both x and y direction and rotation of the crack. All these deviations were part of discussion in [15]. Then their effect was observed on actual carried out experiments.

Calculations were performed for total of 240 combinations of varying parameters [19]. It was considered that Young's modulus does not affect the value of stress intensity factor as the material is linearly elastic. From the results of the calculation an empirical formula was formed. The final formula is dependent on 4 different ratios of parameters. One describes the geometry of the crack. It is the ratio of depth of the crack a and semi-major axis of the elliptical crack c. The second one is the ratio of the depth of the crack and thickness of the specimen t. Third ratio is between thickness and the support radius R_a. Last one is Poisson's ratio. The final formula contains both linear and quadratic terms of the ratios and total of 15 constants (c_{0-14}).

In the last part, an error analysis was performed. For discs above 8 mm in diameter, $0,5$ mm in thickness an uncertainty of approximately 10 % can be achieved if the cracks position does not surpass distance of 120 μm from the center of the specimen [19]. With increasing dimensions of the discs the uncertainty comparable to standard methods is reached. It was also mentioned that the value of Poisson's ratio should be as precise as possible as it has a high impact on precision of this method.

3.4.6 Description of the process of the B3B test

This section covers a guide for the 3B3 test.

In the beginning the apparatus of the B3B test is described. All of the necessary equipment is listed below [1].

- 4 balls of the same diameter
- Stamp that pushes the loading ball into the specimen
- Guide that secures the movement of the stamp
- Block that prevents the guide from toughing the specimen

How these components need to be setup is shown in figure (10) [1]. The red circles represent the points of contact among the supporting balls, specimen and loading ball.

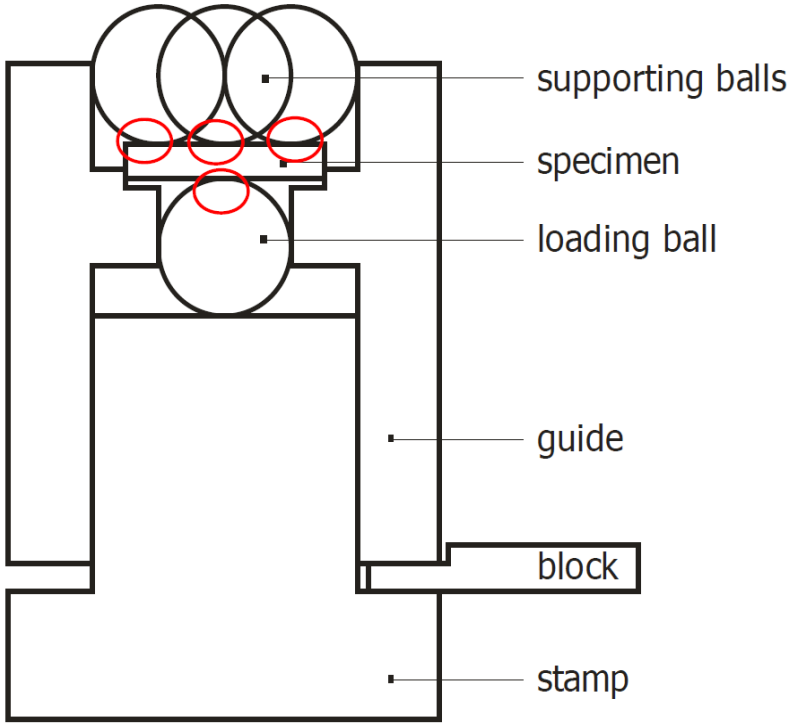

Figure 10: B3B test setup [1].

First step is of course the preparation of the specimen. When the specimen is finished the following operations need to be performed [1].

First the stamp is inserted into the guide. The loading ball is then positioned onto the stamp. The stamp has a small dim in its center so that the loading ball does not slide away from the centre. Specimen is placed onto the loading ball centred by a rim in the guide. Supporting balls are placed on the specimen and kept in position by the inner surface of the guide. The loading ball should be the only point of contact on this side of the specimen. For this the block is used. If these steps were performed correctly the specimen should be able to slightly tilt. With setup finished, this whole apparatus is placed in the testing machine.

The test itself can be described in couple of steps as well. A preload is applied to the specimen using a flat punch [1]. Typical value of the preload is 10 % of the expected fracture load. At this point a check is required to ensure the contact of the supports is correct. At this point the block is removed. If the preload is maintained

the supporting balls may move freely while the loading ball is fixed in its position. Now the load is applied until the failure of the specimen. All balls and fragments of specimen are removed while the stamp and the guide are still connected.

Closer inspection of the fractured specimen is required [1]. Data acquired from specimen with the clear indicators of contact damage cannot be used for final evaluation of the fracture stress.

4 Computational models for the simulation of the B3B test

The type of the modelling used is so-called computational simulation [2]. Simulation in the terms of science and technical application is mimicking a process happening in real life using computers. Its main characteristics are the usage of a certain software, that applies a specific algorithm. This algorithm implements a mathematical theory. In this case it is the ANSYS Mechanical APDL software, that uses Finite element method (FEM) as its mathematical theory.

It was already proven that effect of friction between the balls and the specimen is negligible [9]. Therefore, in all further calculations the punching ball was replaced by a single force and the support balls were replaced by an essential boundary condition, which fixes displacement in the axial direction.

4.1 Models of flat specimens

The flat models represent flat specimens used for the B3B tests. Flat specimen have either the shape of a disc or a plate. The next section is focused on the models of flat specimens.

4.1.1 Model of a flat monolithic disc

In this section the least complicated model is described. It is the model, which takes no curvature into consideration and the model is considered to be monolithic.

The disc specimen is geometrically fully defined by its radius and thickness (r and t). In figure (11) some of the quantities read from an input file are shown.

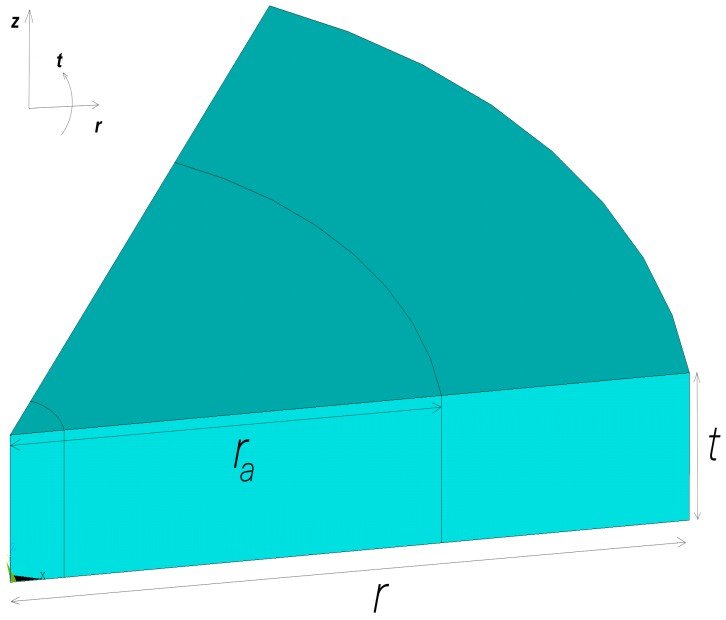

Figure 11: Model of the flatt monolithic disc specimen.

Other required quantities are the material properties (Young's modulus and Poisson's ratio). Material properties are listed in table (1). These quantities are read from an input file. Once the calculation is finished, output values are written into an output text file. Values written are the 1st principal stress at the center of surface tension of the specimen and the f factor for the specific configuration of the simulated test.

The disc specimen is symmetrical, where the axis of symmetry is the same as the direction of the applied force. Due to this property it is possible to model one sixth model of the actual specimen. The best coordinate system for this model is a cylindrical coordinate system with an origin in the bottom center of the specimen. Symmetries such as this are usually desired for numerical simulations, as they reduce the number of unknown parameter, which shortens the time of the computation. Boundary conditions (BC) of the model must respect the applied symmetry. BCs of this model are listed below and are also shown in figure (21) along the FE mesh generated for this model.

- Zero displacement along the axis of symmetry in axial and radial direction of the global cylindrical coordinate system

- Zero tangential displacement of the tangential areas of the model (global cylindrical coordinate system)
- Zero displacement in the direction of the z axis at the location of the support ball

Displacement constrains of both axis of symmetry and tangential areas of the model are required by the implementation of symmetry. In the list above, all BCs only apply to the geometry. The last BC which is necessary to add is the applied loading. Force loading is applied in the middle of the specimen. In case of the disc model only 1/6th of the force F (due to a model symmetry) is applied.

For the simulation, it is required to create a mesh of finite elements. For more precise and faster calculations, it is recommended to use a hexagonal mapped mesh. That means that the elements are all of the same shape and those connected have similar size. In this case it is impossible. Because of this, the volume was divided into 3 smaller volumes of which 2 could be meshed with mapped mesh. Only the last volume, which is the tip of the model (in proximity of the axis of symmetry) is meshed with a free mesh. The FE mesh is depicted in figure (21). Every line was divided according to its length. This allows the model to have a very dense mesh in the center, where the force is applied. On the other side, the part of the model that lies outside of the radius of the supports (r_a) does not need to be meshed densely. The dense mesh in the middle of the model is important as it is the place, where stress is evaluated. If the mesh was not fine in this area, then stress singularity at the place of the applied force would dominate and the value on the opposite side of the model would not be as precise or even completely wrong.

4.1.2 Model of a flat monolithic plate

For the plate specimen, symmetry cannot be used. The reason behind this is that the specimens base is rectangular while the supports are located on a circle. The model created in ANSYS is a lot different from the disc. The model is created from 7 subsequent volumes. Also in this case a smaller circle for free mesh in the center was used The circular area is divided into three same-sized areas each spanning 120 degrees (from 15 to 135, from 135 to 255 and from 255 back to 15 degrees). This

creates three-part cylinder in the middle and outside of that a cylinder with inner radius equal to the radius of the inner cylinder. The last volume is the outer part that creates the outline of the plate. Described situation is shown by figure (12).

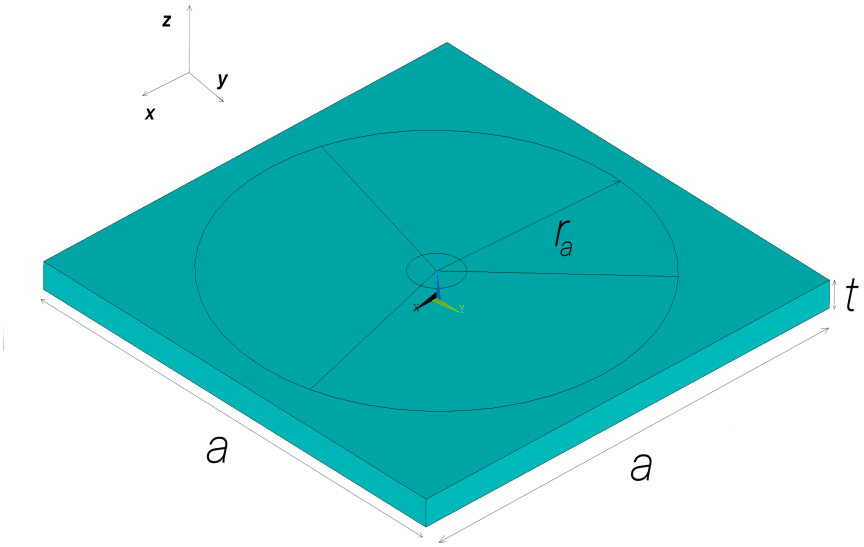

Figure 12: Model of the flat monolithic plate specimen.

The figure also shows the geometric parameters which are necessary for creating the model.

Since the full model had to be used the constraints do not include the effect of symmetry. Displacement constrains used for this model are listed below. BCs of this model are depicted in figure (24) along with the FE mesh.

- Zero displacement on the axis of symmetry in x and y direction of the global Cartesian coordinate system
- Zero displacement it all three locations of the supporting balls

While the first BC is the same as in the case of disc specimen, the second one is applied to 3 different locations. Also this configuration of the simulation is the reason for the implementation of the parameter called 'angle of offset' (AOO). The supports can be located in different places defined by AOO. This allows for many

possible configurations of the supports, all of which would lead to a different results of the maximal stress in the bottom center and f factor of the simulation. Figure (13) shows the parameter AOO.

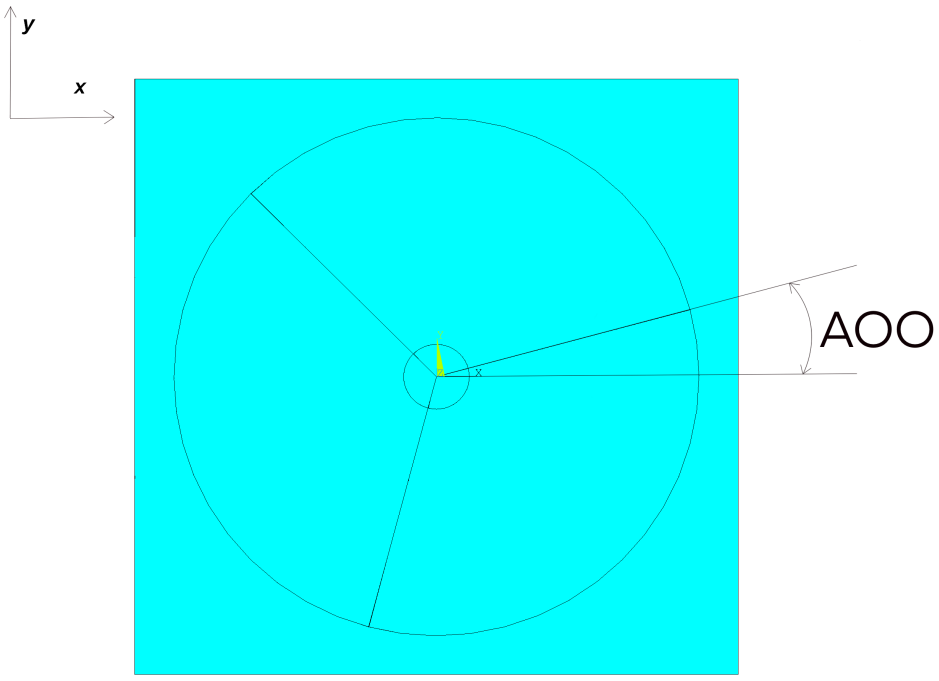

Figure 13: Angle of offset of the model of monolithic plate specimen.

The volumes were created as described so that at least part of the mesh can be mapped. The middle stays unmapped and this time the outer part has to be unmapped as well. The volumes between the center and the outer part are mapped.

The force is applied to the center of the specimen.

4.2 Models of curved monolithic specimens

The calculations for both flat specimen were carried out. The next effect to include is curvature of the specimen. For this part 3 separate macro files had to be created. The first one calculates curved disc specimen. The second one simulates the scenario where the plate is curved but only in one direction. The specimen is basically a cutout of a cone with an inner radius. The last file executes a calculation of a plate specimen curved in both directions. The shape of this specimen is a cutout of a sphere.

In the next chapters the process of creation functional macro files is described.

4.2.1 Model of a monolithic curved disc

The symmetry can be exploited as was in the case of a flat specimen. That is due to the fact that curvature does not effect the tangential direction of the model at all. The only direction affected by the curvature is the z direction.

This type of specimen requires a parameter which describes the curvature. This new parameter is shown if figure (14) as well as the directions of this model.

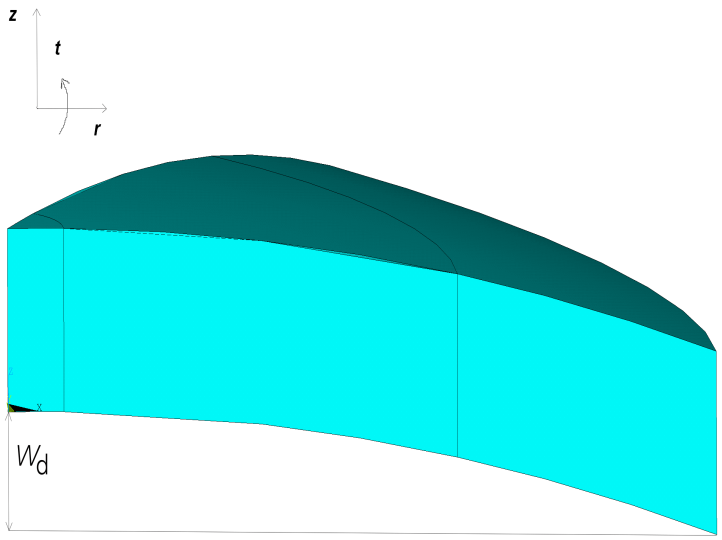

Figure 14: Volumes of the model of the curved disc specimen.

The most reasonable way to include the effect of curvature is to use the parameter w_d (for disc). The curvature can be later evaluated with parameters such as the radius of curvature $\rho\,[\mathrm{mm}]$ or curvature $\kappa\,[1/\mathrm{mm}]$. The relation between radius of curvature and curvature is described in equation (15).

$$\kappa = \frac{1}{\rho} \tag{15}$$

Both of these parameters are better for describing curved lines or surfaces. The parameter w_d is used in the input file instead of the other parameters describing

curvature since it is easily measurable.

The boundary conditions remain the same for this model. The BCs are still listed below for clarity reasons.

- Zero displacement along the axis of symmetry in axial and radial direction of the global cylindrical coordinate system
- Zero tangential displacement of the tangential areas of the model (global cylindrical coordinate system)
- Zero displacement in the direction of the z axis at the location of the support ball

The load is also applied to the top center of the specimen. The value of the load is also unitary. But because of the applied symmetry the value of applied force is divided by 6 as well.

The main difference between this model and the flat one is in calculation preceding the simulation itself. The coordinates for each keypoint needed to be calculated. The keypoints on the edge of the specimen are easily calculated. The change in their z coordinate is simply the value of the parameter w_d. The other two needed values (inner and outer radii) needed to be calculated.

Figure (15) [20] portrays the situation.

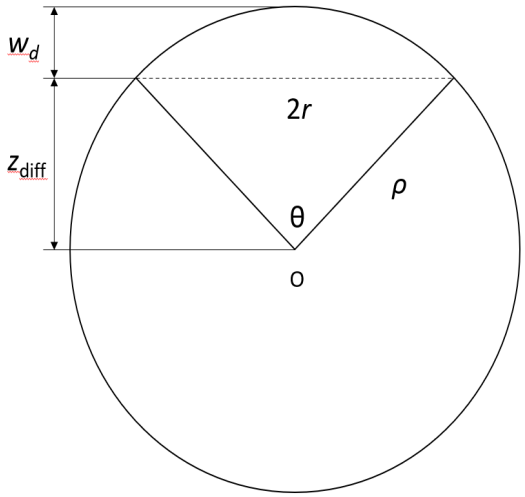

Figure 15: Parameters of a circular arc [20].

Initially the only known combination of parameters is on the outer edge of the specimen and in the center. From those values the radius of curvature was calculated by equation (16) and (17).

$$r = 2\sqrt{w_d\,(2\rho - w_d)} \tag{16}$$

$$\rho = \frac{r^2}{2w_d} + \frac{w_d}{2} \tag{17}$$

This means all other unknown values of KPs in the z direction can be calculated. The reason the radius of curvature ρ is key is that now coordinates of all points of a circle can be obtained from the equation of circle - Eq. (18).

$$(x - x_0)^2 + (z - z_0)^2 = \rho^2 \tag{18}$$

The center point of the circle O has coordinates $[x_0; z_0]$ where $x_0 = 0$ and $z_0 = -\rho$. Since the x values were already determined (radii of both inner and outer arcs) the equation of circle was used to obtain the z values for these KPs.

4.2.2 Model of a monolithic plate curved in one direction

This specimen is curved only around one axis. The axis around which the curvature is considered is the x axis. This model uses the same concept for introducing the effect of the curvature. The distance between the center and the edge of the specimen can be easily measured for this specimen as well. In figure (16) the parameter that includes the effect of curvature (w_{p1}) is shown. Other parameters that are needed for the definition of the model keep their symbols from previous models.

The same system of 7 volumes creating the whole geometry was used. The geometrical model is illustrated in figure (16).

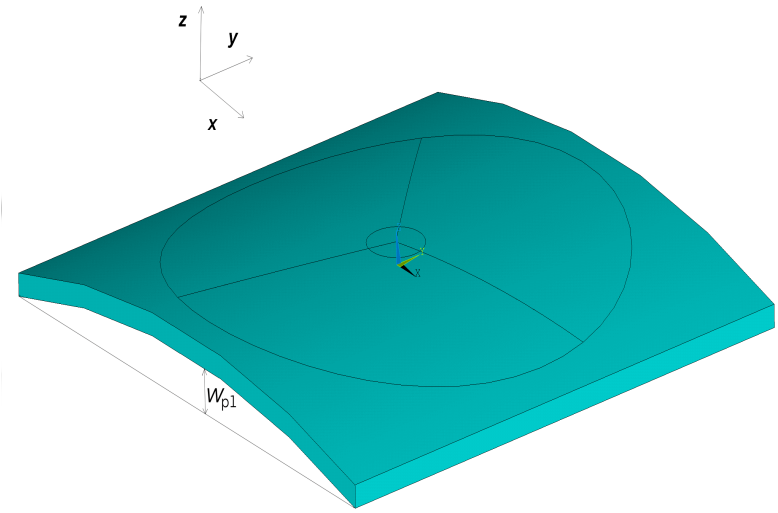

Figure 16: Model of the plate specimen with curvature effect in one direction.

Geometry of the model makes it difficult to easily calculate the locations of keypoints. In the previous case the advantages of symmetry were used. This time the coordinates of the keypoints depend on more than one direction. Another approach taking into account the radius of curvature had to be used. A new keypoint was defined in the negative direction of the z axis at the distance equal to the radius of curvature. This keypoint serves as a tip of a cone. The cone has a tip angle that can be calculated from the input parameters. The formula used to calculate this angle is written in equation (19) [20].

$$\theta = 2 \arcsin \frac{r}{2\rho} \tag{19}$$

The approach involving 7 volumes is maintained which means that the cone is divided into 3 separate partial cones. Each of these partial cones span 120° starting from the angle of offset.

The notation in this equation is already modified to correspond with used variables. The height of this cone is slightly bigger than radius of curvature ρ plus thickness t. Creating intersections between the top and bottom areas of the model and the cone creates the necessary keypoints for creating the geometrical model.

The BCs do not change from the flat specimen as well. This means they were already mentioned earlier but again for clarity reasons are listed below as well.

- Zero displacement of the axis of symmetry in x and y direction of the global Cartesian coordinate system
- Zero displacement in all three locations of all the supporting balls

The load is also applied to the top center of the specimen.

4.2.3 Model of a monolithic plate curved in two directions

The last model of the monolithic specimen is the plate specimen curved in two directions (x and y). Even in this case the parameter that brings the effect of curvature is the distance from the center of the specimen to the side. This time only to the four vertices on the bottom side of the specimen. The system of substantial quantities is therefore the same as in the previous case. The effect of curvature is implemented through a parameter called w_{p2}, which is shown in figure (17).

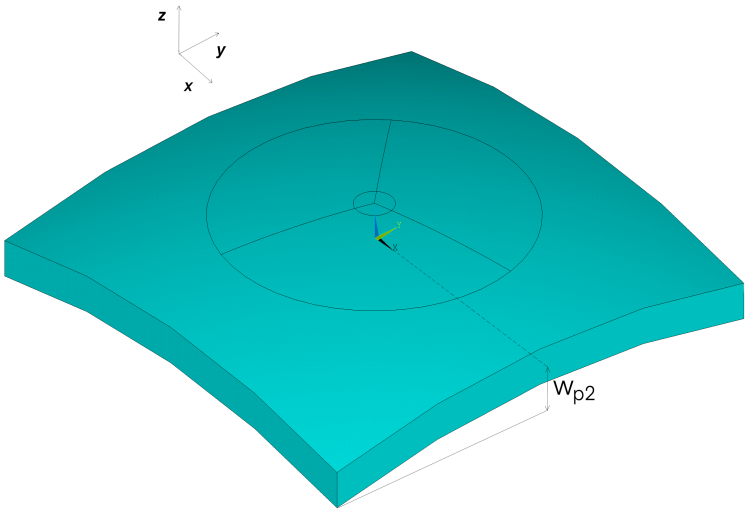

Figure 17: Model of the plate specimen with curvature effect in two directions.

It is important to understand that in each of the curved models the curvature effect is implemented through a parameter that describes the curvature in relation to the geometry of the model. This time it represent the distance from center of the specimen to the 4 vertices in the z direction.

The way the cones were introduced and utilized by the previous model is the same for this model. The boundary conditions remain the same as well. The force was applied to the center of the top side of the specimen.

4.3 Models of curved laminates

The previous models only describe situation where the specimen is monolithic. The effect of having multiple layers in the specimen was now explored for the curved specimens.

When the effect of multiple layers is taken into account, new parameters enter the system of substantial quantities. These parameters are the number representing the number of layers of the laminate (n) and their individual thicknesses t_i.

All created macro files were created directly from those of curved monolithic specimens. For every type of curved specimen 3 new files were created. These new files have manually selected number of layers (3,4 and 5).

The next figures (18), (19) and (20) show the volumes of each model. The disc model is depicted with 5 layers. The plate model curved in 1 direction is depicted with 4 layers and the plate model with curvature in 2 direction with 3 layers. All these three models were created in 3 versions having different number of layers. In each figure the layers are highlighted. Including figures of all of these would not bring any new information.

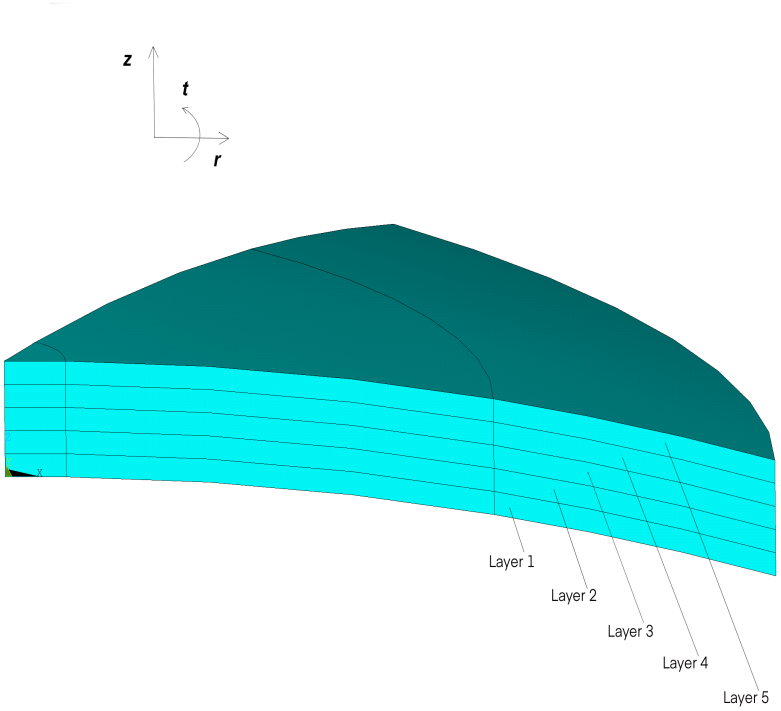

Figure 18: Volumes of the model of the curved disc specimen with 5 layers.

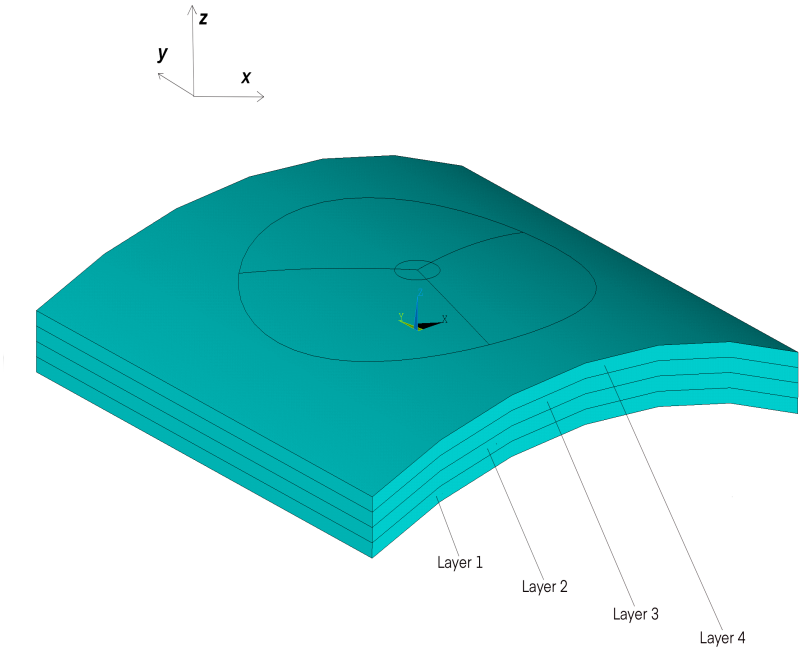

Figure 19: Volumes of the model of the plate specimen curved in one direction with 4 layers.

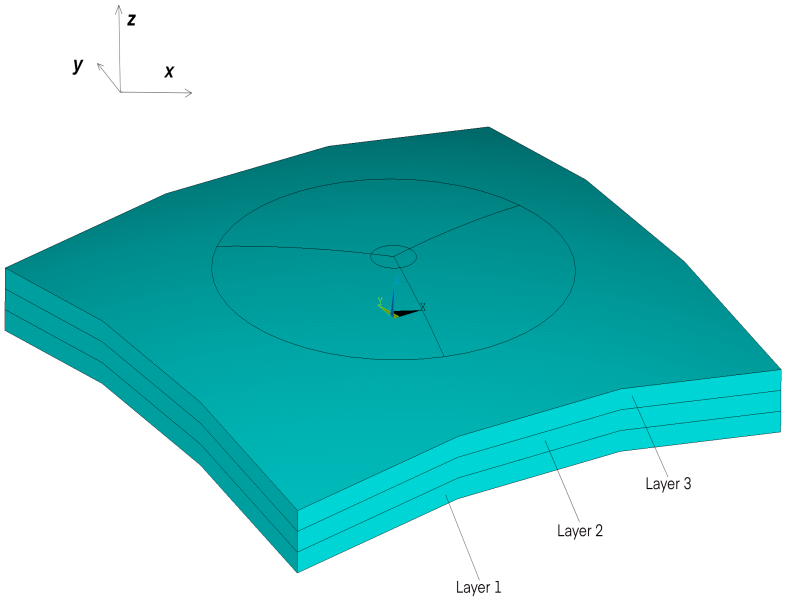

Figure 20: Volumes of the model of the plate specimen curved in two directions with 3 layers.

The input parameters of these models depend on the number of layers as well, since material properties need to be assigned to each layer separately. The process of assigning the material properties to each layer is done inside the macro file. Everything up until this point in each macro file was the same with only the number of KP, lines, areas and volumes increasing with the amount of layers. In the meshing part of the calculation only volumes of specific layer were chosen and assigned a material number corresponding with the parameters in the input file. BC of every model remained the same.

Materials chosen for the laminates are aluminium oxide, which was already used for monolithic models, and tetragonal-zirkonia-toughened alumina. These two materials alternate between layers. In the bottom layer it is always the aluminium ceramic. For any two materials A and B the configurations would for 3 layers be A-B-A, for 4 layers A-B-A-B and for 5 layers A-B-A-B-A. These materials were chosen because their properties are available in literature [21] and [22]. Properties of both materials are listed below in table (1).

Table 1: Material properties of materials considered in th calculations.

Material \ Property	σ_0	E	ν	α
A	645	367000	0,22	$5,81 \cdot 10^{-6}$
B	485	380000	0,22	$6,74 \cdot 10^{-6}$

5 Results of the B3B test simulations

5.1 f factor analysis on a monolithic specimen

After the models were prepared via ANSYS macro, calculations were carried out. The calculated values were 1st principal stress in the center of the bottom side of the model and f factor. Stress values were obtained with loading of a unitary force.

5.1.1 Monolithic disc

In case of the monolithic disc model only several calculations were performed. Besides the input parameters the most interesting effect on the simulation output (f factor and 1st principal stress) is the thickness of the specimen. Values of input parameters are shown in table (2).

Table 2: Considered input parameters for the monolithic disc model.

r	r_a	F
5	3,125	1

The radius of supporting balls is chosen based on the radius of the balls used in the experiment. Only certain values of the radii where the balls are located are available. One of the other common configurations is that the specimens radius is 10 mm and the radius of the supporting balls is $8,7$ mm.

The values of material properties (E and ν) represent properties of aluminium oxide created via 3D printing [22]. Aluminium oxide is one of the most commonly used ceramics.

Realistically the value of the fracture force F_max is different. But the value of f factor would be the same for different values of applied force due to the linearity of the model. This means that the most important value obtained from the calculation is the f factor. It can be shown how its value changes when the specimens properties change.

Now the process of creating this particular model is described. All keypoint locations are defined directly from input parameters shown in table (2). This model uses only 14 keypoints (KP). Seven for the bottom side and seven for the top side.

The locations for these keypoints are the center of the specimen, inner radius that defines the area with unmapped mesh, outer radius (support radius) and the edge of the specimen. After all keypoints were defined, the lines were created. All lines except for the tangential ones are straight. The three tangential lines are simply arcs of the certain radius. The areas created from these lines are all flat. Three volumes were created for the convenience of meshing. After the volumes were created, the next step is to divide the lines for the meshing accordingly. All lines were divided based on their position so that the meshed could be mapped. The meshed model as well as applied boundary conditions are shown in figure (21).

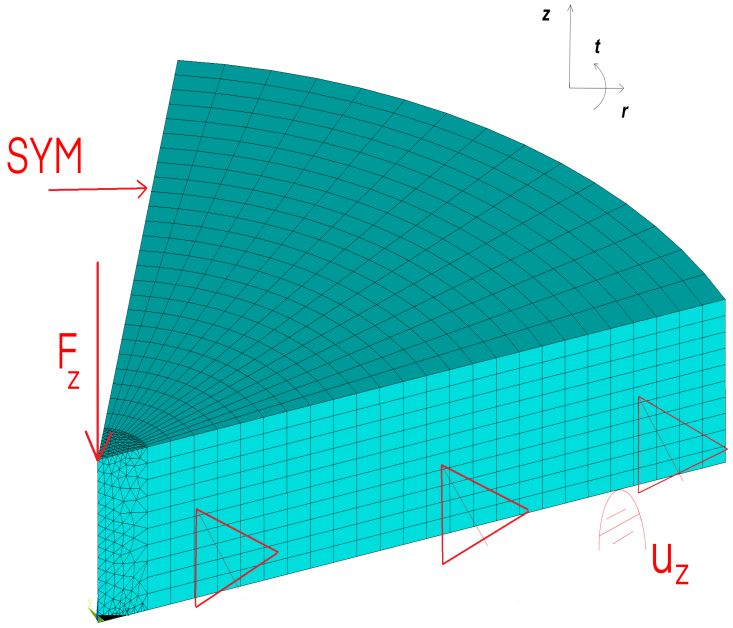

Figure 21: Mesh and BCs of the flat monolithic disc model.

One of the last steps in the preprocessing part is to create the FE mesh. In the present model, quadratic SOLID186 elements were used. One of the advantages of this particular element is ability to create both hexagonal and tetragonal mesh. Material properties of the specimen were assigned to this element.

With all of these steps, the calculation itself can be executed. Calculations were performed for 6 different values of thickness.

The values used for t are $(0,250;\ 0,50;\ 0,750;\ 1,0;\ 1,50;\ 2,0)$ mm.

For these values the stresses, and consequently f factors in the middle of the

bottom side were evaluated. The dependence of both of these output quantities on the thickness of the specimen is shown in figures (22) and (23).

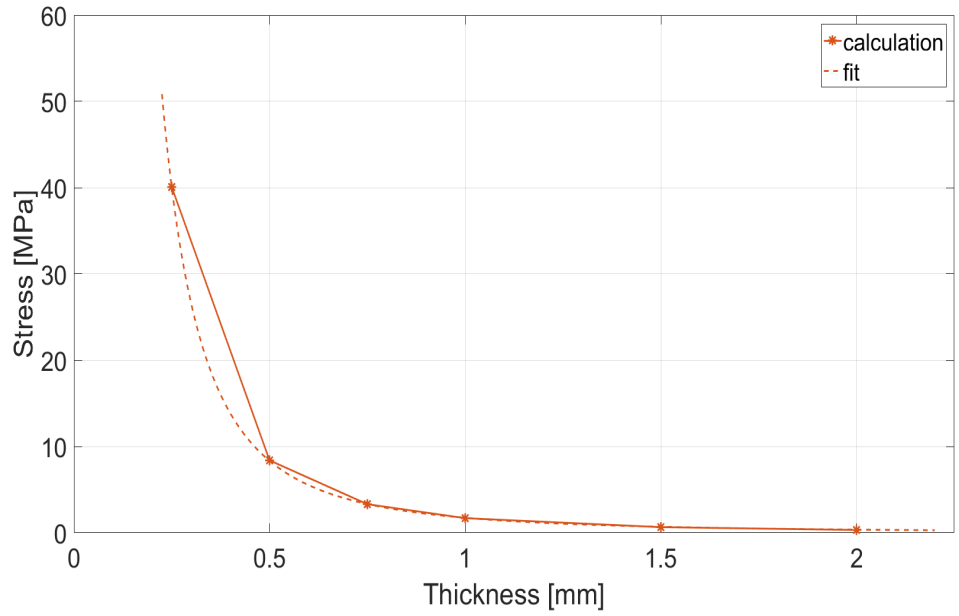

Figure 22: Dependence of the 1st principal stress (loading force $F = 1$ N) on the thickness for a model of the disc specimen with the best fit found for the data.

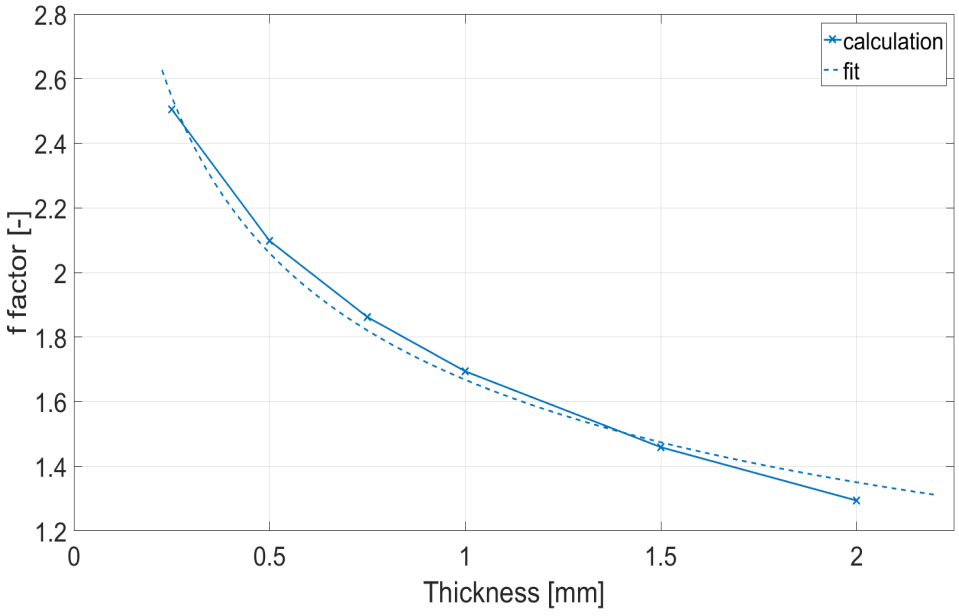

Figure 23: Dependence of the f factor on the thickness for a model of the disc specimen with the best fit found for the data.

While the values in the stress figure do not represent a real carried out exper-

iment, the trend would remain the same for different values of loading force. It is obvious that both values drop with increasing value of thickness. Value of stress is inversely proportional to the square of thickness. This was shown in analytical solution of the 3B3 test described by Börger et. al. [9].

The curve fitting toolbox was used to find the best fit for both graphs. After looking at the graphs the most reasonable type of fit seems to be some hyperbolic curve. A corresponding equation with unknown coefficients is written in the equation (20).

$$f(x) = ax^b \tag{20}$$

The value of the parameter b is expected to be negative so that the fitted curve is a hyperbole. The parameters a is a scaling parameter.

The first attempted fit is for the graph of stress and thickness. Values of parameters a_d and b_d (index d stands for a disc) are listed below.

- $a_d = 1,736$ with 95% confidence boundary being $(1,695; 1,778)$
- $b_d = -2,264$ with 95% confidence boundary being $(-2,282; -2,247)$

Besides from these parameters there are also parameters that evaluate the goodness of a fit. The parameters describing the fit are sum of square estimate errors (SSE), which is also known as residual sum of squares (RSS), R-square and root-mean-square error (RMSE). All of these values range from 0 to 1. For SSE and RMSE the better the fit is the closer are both of these to 0. R-square is the opposite. The closer it is to 1, the better is the fit. All 3 of these values are again listed in table (3).

Table 3: Goodness of the fit for the 1st principal stress in a flat disc model.

Name of the parameter	Value
SSE	0,008423
R-square	1
RMSE	0,04589

From these values it is safe to assume the fit is very good. It also means that a good fit can be expected from the f factor/thickness data.

Since the fit via power curve was successful the same type of fit was also used for the second graph. The values that were calculated from curve fitting toolbox are listed below.

- $a_d = 1,668$ with 95% confidence boundary being $(1,609; 1,727)$
- $b_d = -0.3046$ with 95% confidence boundary being $(-0,3448; -0,2644)$

And the parameters that describe the goodness of the fit are shown in the table (4).

Table 4: Goodness of the fit for the f factor in a flat disc model.

Name of the parameter	Value
SSE	0,00879
R-square	0,9909
RMSE	0,04688

This fit is also very precise. The reason why the R-square is different (but yet still very precise) is that the f factor value is calculated inside of the ANSYS simulation and then written into the output file with limited number of decimal places. This is where the difference could come from.

5.1.2 Rectangular monolithic plate

Plate specimen are not yet quite common in B3B testing. Therefore the dimension of the specimen were chosen to be close to those used in disc calculation. The constant input values are shown in table (5). The same material properties were used.

Table 5: Considered input parameters for the monolithic plate model.

a	r_a	φ	F
10	3,125	15°	1

The edge length a was chosen to be 10 mm to correspond to the radius of the disc specimen. The radius of the supports is the same as for the disc specimen. Material was assumed to be the same as there is no reason for it to be different. The applied

force is also chosen to be 1 N. The reason for this is the same as already mentioned for the disc specimen.

The value of AOO was chosen as stated above as it is the configuration that is used for testing. Nevertheless, the user can set the variable AOO in the created code arbitrarily to simulate all possible configurations.

The process of the model of the plate specimen creation was not as simple as the disc one. This model requires 22 keypoints in total (11 for both sides). One KP is located in the center of the specimen. 3 KPs are located at the radius defining the end of unmapped mesh. Their angles in the main coordinate system are the angles of supporting balls. Another 3 points are exactly at the locations of the support balls (radius r_a). Last four points are the vertices of the square (plates sides shape). The FE mesh is shown in figure (24).

Lines were created from these keypoints. All lines are again straight except for those on the radii of end of mapped mesh and supports. But due to the the more complicated nature of this model, the number of required lines is much higher. All areas divide the specimen into 7 volumes. The same process of setting the number of division on lines was applied as in the case of disc specimen. All lines were divided according to their position. The meshing process is unfortunately more complicated in this case. Three volumes forming the inner conical shape are created with free mesh. Other three volume posses the conical shape with nonzero inner radius. One final volume forms the outer part of the specimen.

Similarly to the disc specimen the material properties were set based on table (1). Element type SOLID186 was used again. The boundary conditions mentioned before were applied in this step. Visual interpretation of the boundary conditions along with the generated FE mesh are shown in figure (24).

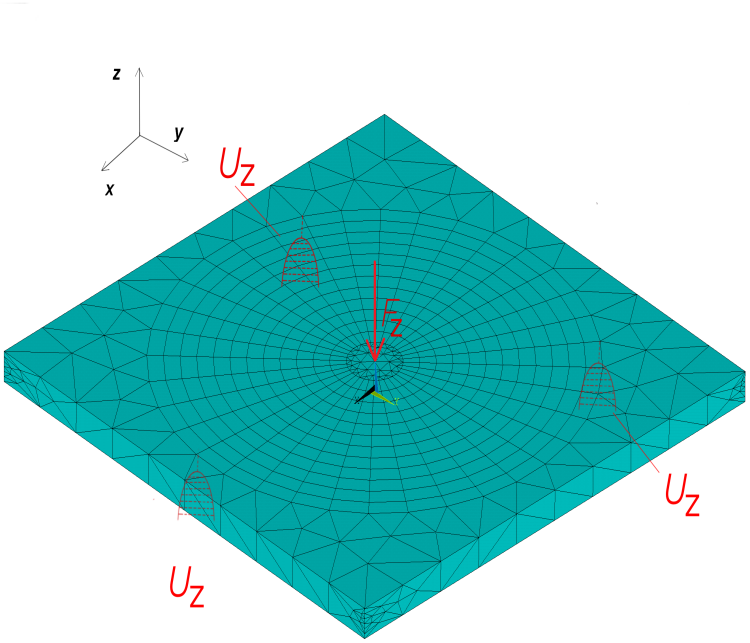

Figure 24: Mesh and BCs of the flat monolithic plate model.

The calculations were performed for the same values of thickness as in the case of disc specimen $(0,250;\ 0,50;\ 0,750;\ 1,0;\ 1,50;\ 2,0)$ mm.

Relation between the stress and thickness depicts the figure (25) and between the f factor and thickness the figure (26).

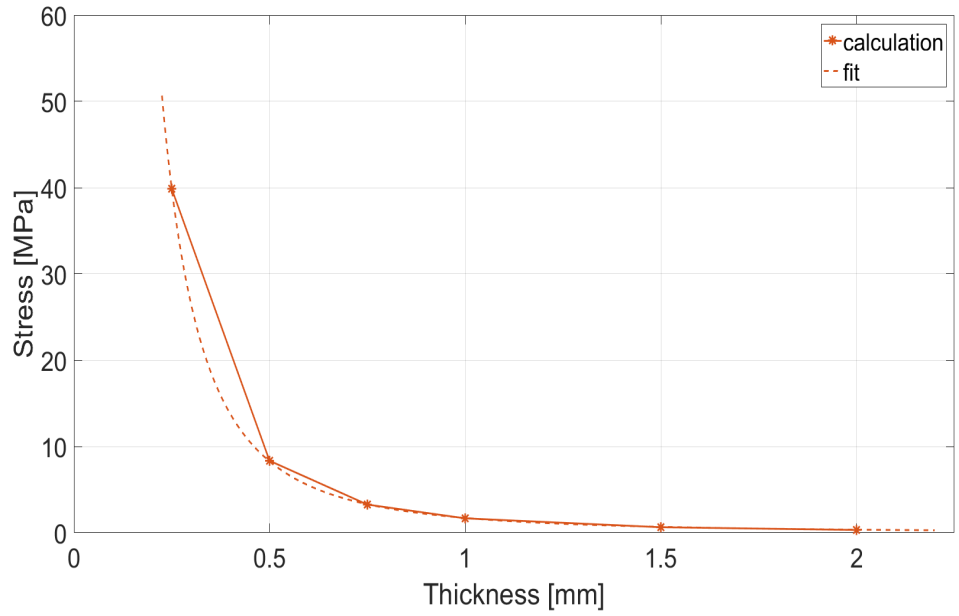

Figure 25: Dependence of the 1st principal stress (loading force $F = 1$ N) on the thickness for a model of the plate specimen with the best fit found for the data.

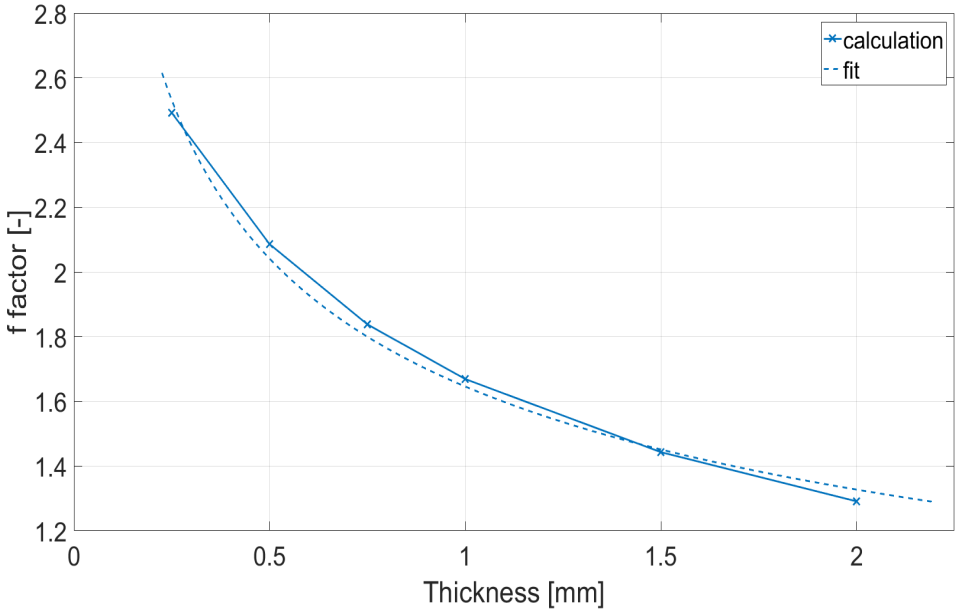

Figure 26: Dependence of the f factor on the thickness for a model of the plate specimen with the best fit found for the data.

Due to the dimensions of the specimen corresponding with the disc specimen, all calculated values are quite similar to the calculations performed for the disc specimen.

Again a hyperbolic trend can be observed on both figures. The same formula as in equation (20) was used to fit through these data.

Values of coefficients a_p and b_p (p for plate) are listed below.

- $a = 1,7200$ with 95% confidence boundary being $(1,672; 1,769)$
- $b = -2,268$ with 95% confidence boundary being $(-2,288; -2,247)$

The goodness of this fit (SSE, R-square, RMSE) is shown in table (6).

Table 6: Goodness of the fit for the 1st principal stress in a flat plate model.

Name of the parameter	Value
SSE	0,0114
R-square	1
RMSE	0,05337

The result is similar to the disc specimen. The fit is very precise.

The next fit was performed for the f factor. Coefficients a_p and b_p and their 95 % confidence boundaries are listed below.

- $a = 1,646$ with 95% confidence boundary being $(1,589; 1,704)$
- $b = -0.3105$ with 95% confidence boundary being $(-0,3502; -0.2708)$

Table (7) evaluates the goodness of this fit.

Table 7: Goodness of the fit for the f factor in a flat plate model.

Name of the parameter	Value
SSE	0,008385
R-square	0,9915
RMSE	0,04578

These values indicate another precise fit of the data. It is now reasonable to assume that the dependence of the values of stress and f factor on the thickness of a specimen in a B3B test of both disc and plate shaped specimen is hyperbolic.

5.2 f factor analysis on a curved specimen

All of the calculations of models of curved specimens were dependant on 2 parameters. These parameters are thickness t and curvature κ. The curvature of all specimens is limited by the supporting balls. If the curvature of the specimen is too big the configuration of the test would change since the supporting balls may move. The critical curvature κ was calculated to be around $0,025\,1/\text{mm}$. This corresponds with the minimal radius of curvature ρ to be around $40\,\text{mm}$. This new parameter is called the normalized curvature. It simply converts the value of curvature into percents. These percents represent how close is the value of the curvature to the the maximal curvature. The results are evaluated as functions of normalized curvature.

5.2.1 Curved monolithic disc

The calculations with curved specimen are more time demanding than those with the flat models. This is due to the effect of curvature. There need to be more calculations then for the flat models. For each used value of thickness t, a total of 6 calculations with different value of w_d were performed. The table (8) shows all parameters describing curvature and how they are related. Chosen values of the normalized curvature range from 15 % to 90 % with increments of 15.

Table 8: Parameters describing curvature.

Normalized curvature [%]	Curvature κ [1/mm]	Radius of curvature ρ [mm]
15	0,002	555,6
30	0,007	138,9
45	0,011	92,7
60	0,014	69,5
75	0,018	55,7
90	0,022	46,4

The input parameters such as dimensions of the specimen or material properties are the same as in case of the flat model.

The main difference between these two models are the lines of the model. Only the lines connecting the bottom side and the top side are straight. The lines in

tangential direction are not straight but remain the same. The lines in the radial direction are now also subjected to the effect of curvature. Even thought the normalized curvature was introduced, its use in preprocessing part of the calculation was not derived in this work. That means the lines in the radial direction are created by a command for creating the arc of a circle. It uses the radius of curvature ρ calculated from the distance between the center of the disc to its edge w_d.

After the lines are created all the areas are simply created from the closed loops of the lines. The same applies for volumes.

The lines are divided the same way as in the case of the flat model to ensure the mapped mesh on both outer volumes. The center near the tip of the specimen is meshed with free mesh.

Element type SOLID186 was used. All boundary condition were now assigned and the calculation was executed.

This process was repeated 36 times in total for all configurations of thickness and curvature. The value of f factor decreases with both increasing thicknesses and increasing curvatures. The values for normalized curvature equal to 0% were taken from the calculations performed for the flat specimen. Figure (27) shows the relation between curvature and f factor for the different values of thickness.

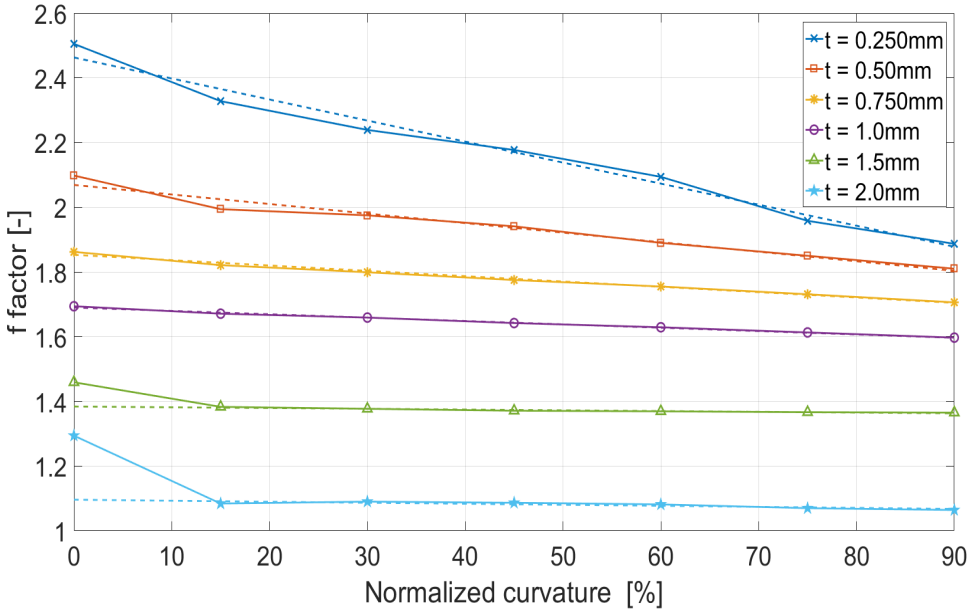

Figure 27: Values of f factor for various curvatures and thicknesses of a model of the disc specimen (full lines) and best fits found for the data (dashed lines).

All the trends seem to be similar. Slowly decreasing with increasing value of normalised curvature. The curvature affects the value of f factor more if the specimen is thinner. Meanwhile for the thicker variants of the calculation (1-2 mm) after the drop from no curvature to 15 % is still notable the other values drop very slowly or not at all.

The trends for stresses are similar thanks to their direct relation to f factor. For example the graph for thickness $t = 0,750$mm is shown in figure (28).

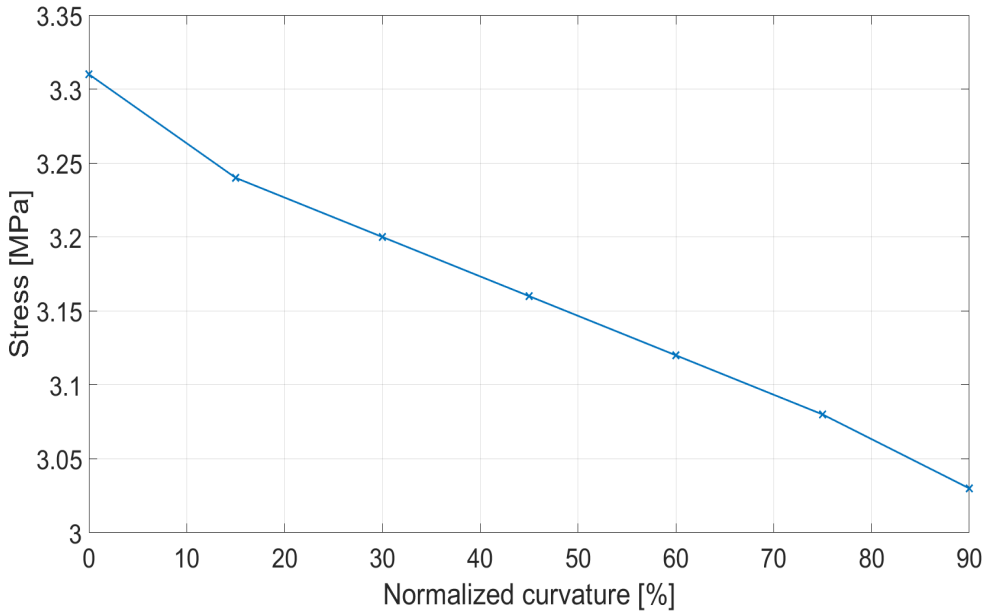

Figure 28: Values of 1st principal stress for different curvatures in a disc model with $t = 0,750$ mm and with a unit force load.

The best fit for the f factors seem to be linear for the first four thicknesses.

Table (9) shows the goodness of linear fits for these thicknesses. In this table both of the coefficient of a line are written. The coefficient a represents the slope of a line and b is a constant term - Eq. (21).

$$f(x) = ax + b \tag{21}$$

Table 9: f factor fits for a curved disc model.

Thickness t	R-square	SSE [-]	a	b
0,250	0,9821	0,004875	-0,0065	2,463
0,50	0,9666	0,00188	-0,00295	2,069
0,750	0,99	0,00017	-0,00165	1,853
1,0	0,9954	$3,1 \cdot 10^{-5}$	-0,00104	1,69
1,50	0,9258	$1,72 \cdot 10^{-5}$	-0,0002339	1,384
2,0	0,7596	0,00012	-0,000316	1,096

For the last two thicknesses there seems to be a significant drop between 0 and 15 percent of curvature. This creates a situation in which the linear equation of the fit does not represent the results from other calculations Excluding the values causing this problem results in much more accurate fit.

In the last case even after excluding the first point the fit does not reach the precision of the previous examples. This might be caused by a numerical error since the value of f factor for the lowest used curvature is lower than the next two values.

The important thing to notice in all of the fits is that the coefficient describing the slope is small, meaning the effect of curvature only slightly decreases the value of the f factor.

5.2.2 Plate curved in one direction

The number of keypoints of this model is the same as for the flat specimen. The main difference is the way they were created. The coordinates of the vertices of the plate were easily calculated straight from the input variable w_{p1} using the formula in equation (17). The lines parallel to the y axis of the main coordinate system remain straight - see figure (16). Those parallel to the x axis were created as arcs with the radius of curvature ρ calculated from w_{p1}. Areas were created from the arcs and straight lines. In the first step whole surfaces connecting the vertices on top and bottom are created. ANSYS provides command AINV that executes Boolean operation of intersection on an area and a volume. It is therefore capable of creating the intersection of the curved areas with the conical volumes. In total 6 conical volumes had to be created to maintain the approach of 7 volumes.

The areas and volumes used in the intersection operation were deleted leaving only the new areas. This was done in order to create areas forming the outer part of the plate from its vertices while the lines on the edges of intersected areas form a close loop. All lines now closed loops so that the areas not yet formed can be added. At last, from all areas the 7 volumes were created - figure (16).

The material properties and element definition remain the same for this calculation.

The calculation was performed 36 times and the f factor graph created is seen in figure (29).

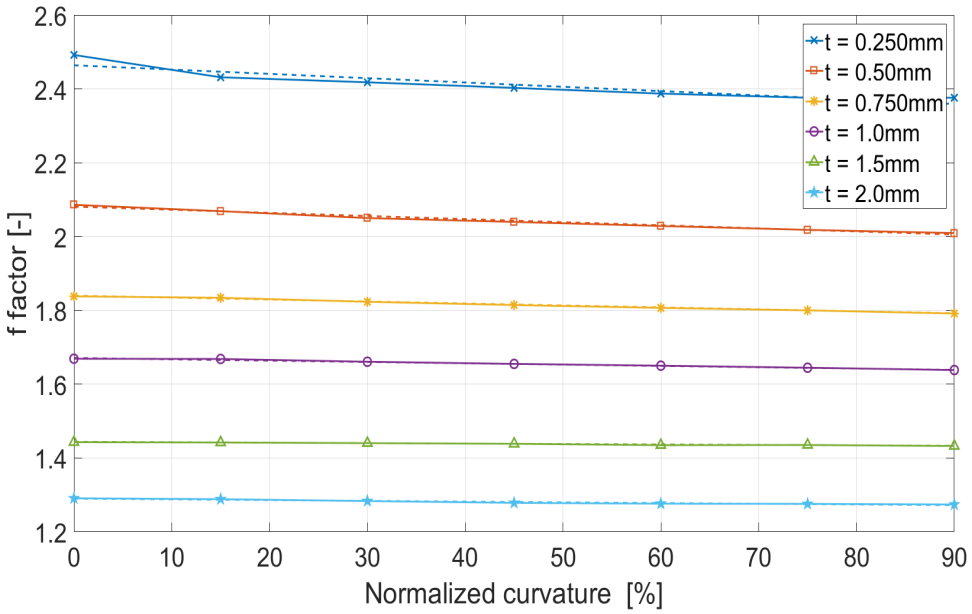

Figure 29: Values of f factor for various curvatures and thicknesses of a model of the plate specimen curved in one direction (full lines) and best fits found for the data (dashed lines).

For this model it seems that the effect of curvature is less impactful. For thickness higher than 0,750mm all of these trends seem to be not only linear but also constant. The values of f factor for normalized curvature of 15% are in some cases higher than for the flat plate but the difference is minimal and is probably the result of numerical error.

For the results of the three thinnest models a fit was performed. These fits are linear as in the case of curved disc. They are described the same way as in the previous chapter - table (10).

Table 10: f factor fits for a plate model curved in one direction.

Thickness t[mm]	R-square	SSE [-]	a	b
0,250	0,8468	0,001546	-0,001165	2,464
0,50	0,9799	$9,1 \cdot 10^{-9}$	-0,00084	2,081
0,750	0,9936	$1,15 \cdot 10^{-5}$	-0,00053	1,84

Once again the stress values correlate with the f factors. As example the stress values for the specimen with thickness $t = 0,50$mm is shown in the figure (30).

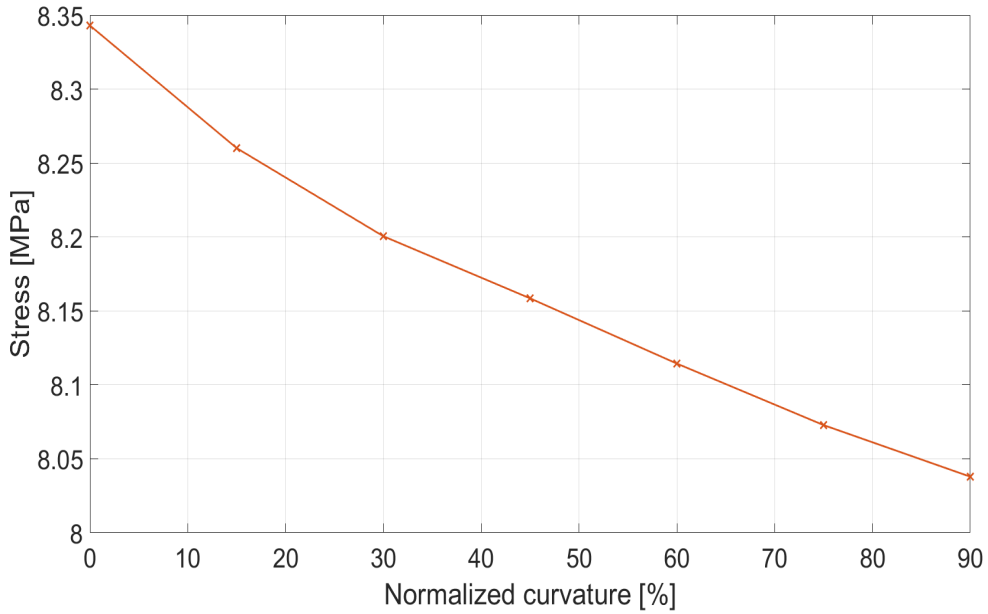

Figure 30: Values of 1st principal stress for a plate specimen curved in 1 direction with $t = 0,50$ mm and with a unit force load.

5.2.3 Plate curved in two directions

This model was created similarly to the plate model with curvature in only one direction. Now both directions include curved outer edges. That means all lines connecting vertices of the plate are curved with the radius of curvature ρ calculated from the input parameter w_{p2}. Once again the approach of creating some of the areas through intersection of cones and the top and bottom areas.

The values of f factor for different curvatures and thicknesses are shown in figure (31).

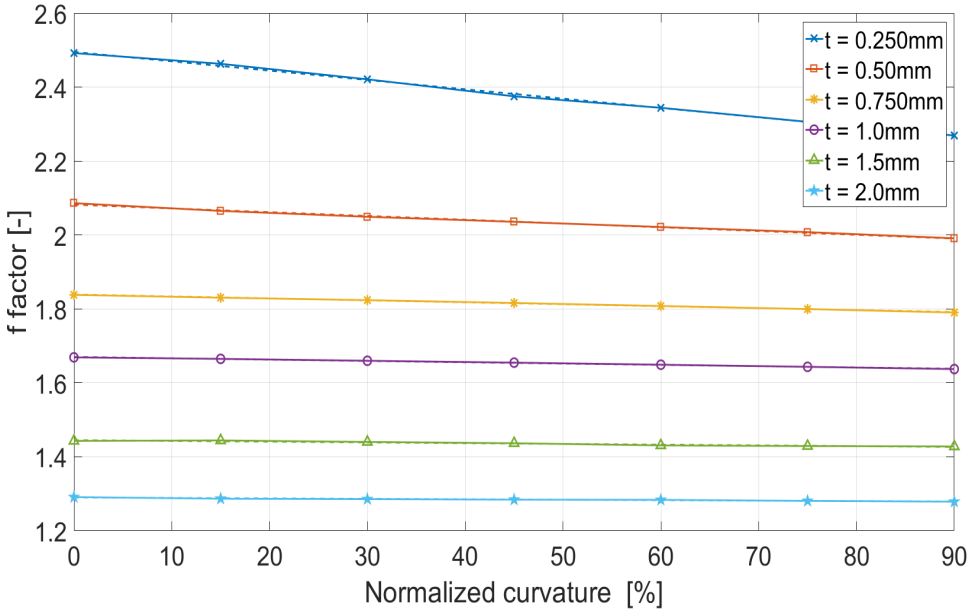

Figure 31: Values of f factor for various curvatures and thicknesses of a model of the plate specimen curved in two directions (full lines and best fits found for the data (dashed line).

All of these lines follow the same pattern as in both previous cases. For the models with highest thicknesses the value of f barely changes with increasing curvature.

The ranges of f factor values are small for thicker specimen. For this reason again only the three thinnest model were fitted. The linear fit was chosen as well. Table (11) shows the parameters of the fits.

Table 11: f factor fits for a plate model curved in 2 direction.

Thickness t[mm]	R-square	SSE [-]	a	b
0,250	0,9978	$8,9 \cdot 10^{-5}$	-0,002524	2,495
0,50	0,9957	$2,8 \cdot 10^{-5}$	-0,001018	2,082
0,750	0,9975	$4,4 \cdot 10^{-6}$	-0,000526	1,839

Also in the case of a plate curved in 2 directions linear relation between f factor and curvature is achieved.

5.3 f factor analysis on a curved laminated specimen

The process for evaluating the relation between curvature and f factor remains the same. For this reason only the configurations depicted in figures (18),(19) and (20) and described in section 4.3 were evaluated. The applied boundary conditions remain the same for all the models. The difference is that the boundary conditions of the z axis now have to be assigned to multiple lines corresponding with number of layers in both plate and disc models. Furthermore, all of boundary conditions have to be applied to all layers.

5.3.1 Laminated curved disc

The disc model with 5 layers is similar to the monolithic model. Since instead of 2 sides (bottom and top) it uses 4 interface surfaces between each layer and bottom and top side aw well total of 42 KPs had to be used. According division of lines by their length was used this time as well. The graph of all the f factor vs. curvature is shown in figure (32).

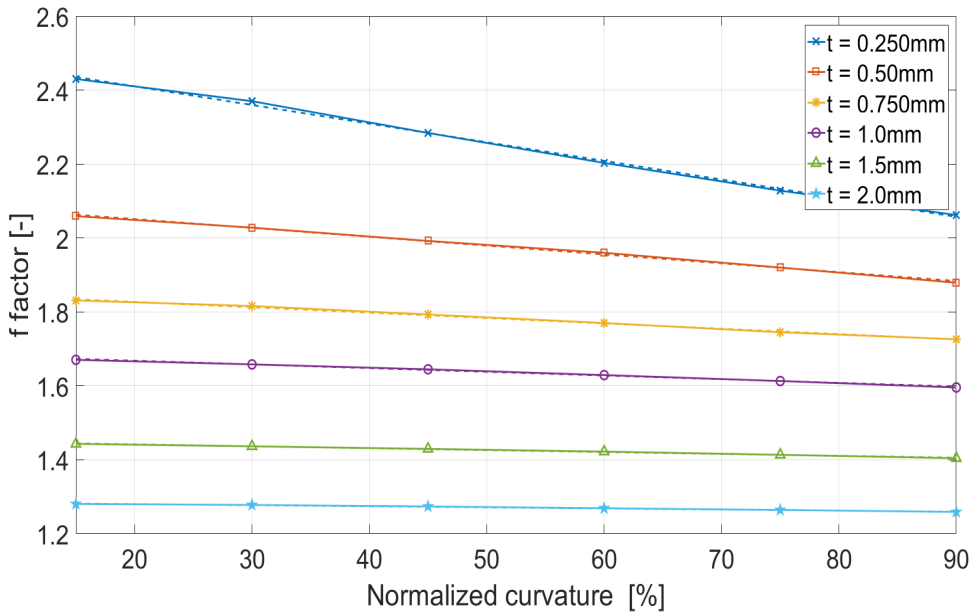

Figure 32: Values of f factor for various curvatures and thicknesses of a model of the laminated curved disc with 5 layers (full lines) and best fits found for the data (dashed lines).

The effect of multiple layers is noticeable on the values themselves since the

second material has different material properties. The trends however remain the same. All of the calculated data again suggest the relation is linear. The decreasing aspect is in this case little more apparent. Again for some of the values of thickness (this time for different values) a linear fit was performed and its parameters are shown in table (12).

Table 12: f factor fits for a disc model laminate with 5 layers.

Thickness t[mm]	R-square	SSE [-]	a	b
0,250	0,9979	0,00021	-0,005042	2,511
0,750	0,9959	$3,4 \cdot 10^{-5}$	-0,00145	1,856
1,5	0,9954	$4,8 \cdot 10^{-6}$	-0,000515	1,452

The fit of f factor curves for laminates of thickness 0,25 and 0,75 is quire similar to those by their monolithic counterparts. Even in case of laminates it seems that f factor has a linear dependence on curvature.

5.3.2 Laminated plate curved in one direction

Conical approach described in section 4.2.2 of creating the necessary intersections proved to be useful even in case of laminates. The cones were deleted after every Boolean intersection. This means they had to be recreated for every layer which made the computation slightly more time demanding. But thanks to the simple nature of the geometry the time increase of the calculation is in seconds. The graph for this configuration shown in figure (33).

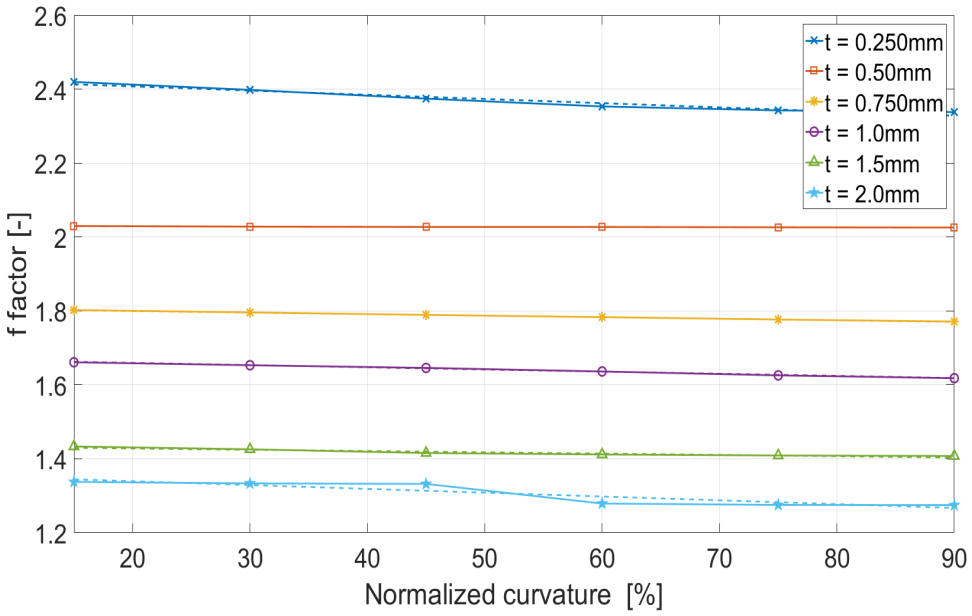

Figure 33: Values of f factor for various curvatures and thicknesses of a laminated plate with 4 layers curved in one direction (full lines) and best fits found for the data (dashed lines).

This time an unexpected jump can be observed for the thickest specimen. This drop in the value occurred during multiple calculations. Preceding values follow linear trend as well as those after. In the case of the different thicknesses the trends appear to be linear as in all other cases.

Fits were performed once again only for half of the values of thickness. Specifically for those used in the model describing the monolithic version of this model. Those values are shown in table (13).

Table 13: f factor fits for the model of the laminated plate model with 4 layers curved in one direction.

Thickness t[mm]	R-square	SSE [-]	a	b
0,250	0,9528	0,00251	-0,001135	2,43
0,50	0,9400	$6,2 \cdot 10^{-7}$	$-4,95 \cdot 10^{-5}$	2,030
0,750	0,9992	$5,6 \cdot 10^{-7}$	-0,000416	1,808

The parameters describing the goodness of the fit are better for laminate than for the monolithic version in 2 out of 3 of these fits. Fit for thickness $t = 0,50$ mm is

slightly worse. Its b coefficient is close but in this particular case the slope is lower. Both other fits are close to the ones created for monolithic version of this model. Other values also follow the linear decreasing trend.

5.3.3 Laminated plate curved in two directions

The last model described in this section is the plate model curved in 2 directions with 3 layers. The creation of this model also copies its monolithic partner. Again with the usage of the cones all curved areas were created. Once the according material properties were assigned to their layer and the boundary conditions were applied, the calculations were performed. Relation between f factor and curvature for this particular configuration is portrayed in figure (34).

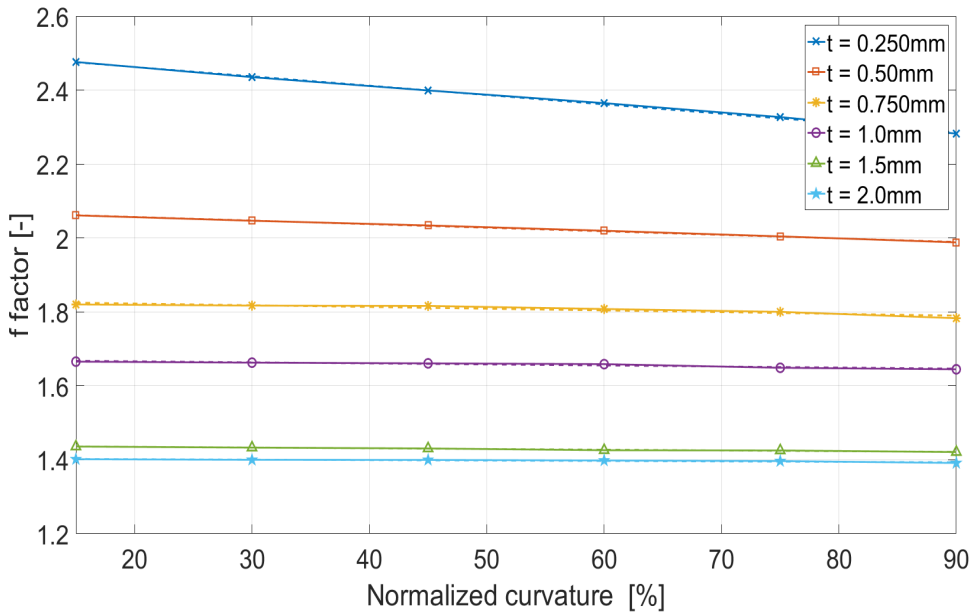

Figure 34: Values of f factor for various curvatures and thicknesses of a laminated plate with 3 layers curved in two directions (full lines) and best fits found for the data (dashed lines).

Even for the last shown model the trends remain linear. The fits and their parameters show this in the table (14). The values of thickness are again chosen to be the same as for the monolithic model.

Table 14: f factor fits for the model of the laminated plate with 3 layers curved in two directions.

Thickness t[mm]	R-square	SSE [-]	a	b
0,250	0,9984	$3,9 \cdot 10^{-5}$	-0,002527	2,513
0,50	0,9985	$5,5 \cdot 10^{-6}$	-0,0009642	2,076
0,750	0,8725	0,00012	-0,0004667	1,832

Even though the R-square is not as high its values are very close to those in the monolithic specimen. The same applies to the other two fits. It is safe to assume that all of the curved laminates follow the linear relation between f factor and curvature. All of the performed fits represent the calculated data with very good precision.

5.4 Incorrect evaluation of f factor in laminated specimen

In previous section it was shown how the laminated specimens behave with the effect of curvature. The dependence of f factor on curvature was shown to be linear as well.

While evaluating tests carried out on laminated specimens, there is potential for inaccurate determination of the f factor. This section describes how this could be performed.

If the outer layers of the specimen are thin, the value of 1st principal stress on the bottom of the second layer (from support side) is only slightly lower than the value of 1st principal stress on the bottom of the specimen. Material of neighbouring layers are different in laminated specimens. The material of the second layer has significantly lower value of characteristic strength σ_0. Even though the mechanical stress is higher at the bottom of the first layer it does not reach the value of its characteristic strength. Meanwhile the stress in the bottom of the second layer could surpass the characteristic strength of the second material. This would result in the initiation of failure on the interface of the bottom two layers. This would occur under load that has smaller value than it would have had if the failure occurred at the bottom of the first layer.

For the means of demonstration the model of the disc specimen with five layers was used. The model was subjected to a loading force $F = 350$ N. Total thickness was set to 1mm. Thickness of the first layer was set to $0,075$ mm. For this specific configuration the first principal stress was calculated. Table (15) shows the values of stresses as well as characteristic strength of the materials of the bottom two layers.

Table 15: Stress values in different layers in a model of laminated disc specimen subjected to load of $F = 350$ N.

Location \ Quantity	Material	σ_1	Characteristic strength	Fracture
Bottom of 1st layer	A	619,5	645	No
Bottom of 2nd layer	B	494,9	485	Yes

This table shows, that for a specific configuration of layer thicknesses it is possible for the specimen to break at a interface of two layers. This could in practise result in an inaccurate determination of the f factor.

In this case, the thicknesses of the first layer was set to less than 1/10th of the whole specimen. This is caused by similar values of Young's modulus as well as characteristic strengths. If the laminated specimen is composed from different materials, the thickness of the first layer for which this effect occurs could be higher.

5.5 Effect of residual stress in laminated specimen

This part of the thesis describes the effect of residual stress in a laminate from materials with two different values of thermal expansion coefficients α. This effect is important for the layered materials. When the residual stresses become high enough, the specimen could break first on the interface of two layers rather than on the bottom.

Furthermore the value of f factor obtained from a test performed on a specimen with residual stress could be misleading. The real value of f factor could be both higher and lower than measured once the effect of residual stresses is omitted. This would cause error in evaluation of the Weibull modulus of the specific material.

Effect of residual stress is introduced separately from the the calculations in ANSYS. For this purpose a MATLAB script was used. Since this script is made

for plate specimens a macro file calculating a laminated plate model of the B3B specimens was used. The residual stresses were applied separately. Applying them inside ANSYS calculations could result in undesired strains in the model which would have negative effect on the evaluated stresses and f factors evaluated in previous chapters. The stress and f factor would also not scale properly for increasing value of loading force.

These effects are shown on 3 different configurations of a symmetric laminate. Symmetric laminate was chosen because the residual stresses are constant along the layers thickness which results in clearer demonstration of the effect. The specimen was considered to be flat.

The same materials as in previous chapters were used. For this demonstration it is necessary to include the values of the characteristic strength of the materials. These values are listed in table (1).

The coefficient of thermal expansion (CTE) α is necessary for this calculation. Its value is not constant but changes with temperature. Measurements are in most cases capped at 1000°C [21]. Since ceramics are sintered at much higher temperatures the use of extrapolation is required. Commonly for technical purposes an average value is used. This average value is calculated as difference in strain over difference in temperature. Its values for ceramic materials lie in a range of roughly $5,0$ to 15 MK^{-1} [12]. Because it describes materials behaviour in relation to temperature change (not absolute value of temperature) its unit can differ in literature. Used units are K^{-1} or $^{\circ}\mathrm{C}^{-1}$.

Residual stresses are the result of sintering individual layers together and their subsequent cooling [22]. Since the layers have different value of CTE residual stresses are developed as a consequence of the desire of the layers to change volumes differently.

5.5.1 1st configuration of layers

In sense of laminates symmetrical configuration means it is composed out of odd number of layers. The middle layer is symmetrically distributed above and below the neutral layer meanwhile every other layer finds a counterpart of the same thickness in the other direction of the z axis [8]. This is depicted in figure (35) for 3 layers.

In the table (16) the configuration of the layers thicknesses are described. All other input variables correspond with those used for a model of a flat monolithic plate.

Table 16: Thicknesses of the 1st configuration of layers.

Layer thickness	Value
t_1	$0,25$ mm
t_2	$0,5$ mm
t_3	$0,25$ mm

Even though 3 layers are used, only 2 different materials were defined. Bottom and top layer are the same material. The material of the outer layers has smaller characteristic strength. The material A in the table (1) is used to model the middle layer. The layer thicknesses were chosen and are different for the next two configurations.

The applied force no longer has unitary value. This time the f factor is not the main focus. Force value was chosen such that the stresses on the bottom of 1st and 2nd layer have specific values to demonstrate the negative effect of residual stress.

The values of CTE of both materials were mentioned in table (1).

These values are approximate due to the amount of uncertainty. For example the exact stress-free temperature is unknown (estimated around $1400 - 1500°$ C). The room temperature where the test is eventually performed may also vary. One last inaccuracy lies in extrapolation of dilatometry measurement far beyond their range. All these reasons result in possible error of every estimation of CTE up to ± 1 MK^{-1}.

From the initial calculation in ANSYS, values of 1st principal stress on the bottom of the first two layers were obtained. These values are listed with corresponding residual stresses in table (17).

With specific values of CTE, material properties mentioned earlier and the thicknesses of the specific layers the MATLAB script was run. The effect of the cooling after sintering the layers together results in residual stresses. For this set of input parameters the resulting residual stresses on each layer are shown in figure (35).

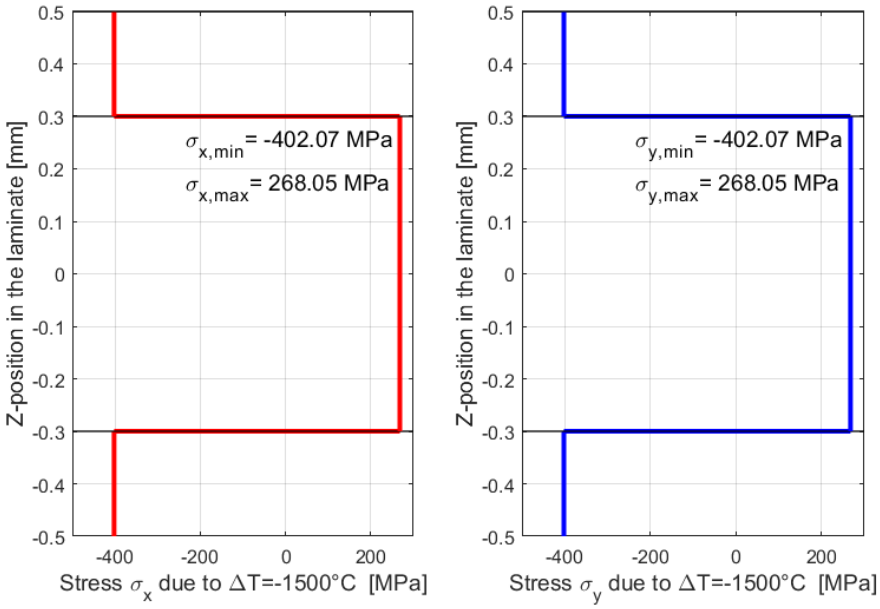

Figure 35: Values of residual stress over the thickness of the laminate in both directions (1st configuration).

Figure includes both x and y direction. But since the materials in discussion are both isotropic both values are the same for each layer. This means that this value of stress is also the 1st principal stress. Thanks to this the values obtained from ANSYS can be directly added to the residual stress values (residual stress = σ_{RES}).

Table 17: Different stresses of the 1st configuration of layers.

Location \ Stress	σ_1	σ_{RES}	σ_0	Total
Bottom of 1st layer	767,87	-402,07	485	365,82
Bottom of 2nd layer	408,26	268,05	645	676,31

From this table a few interesting things can be observed. The value of principal stress is higher at the bottom of the first layer, because of the nature the load. Meanwhile the value of the residual stress is higher in the layer in the middle since its CTE is lower. Without the effect of residual stress the specimen would have cracked just under mechanical load since the value of 1st principal stress surpasses the characteristic strength in this part of the specimen. On the other hand the stress at the bottom of the 2nd layer does not reach the value of the characteristic strength of its material.

But after the inclusion of residual stress, the bottom layer is subjected to compression and the middle to tension. After the load is applied the stress in the bottom layer starts getting lower. The residual stress in this layer works against the load. In the middle layer the load works with the load.

This allows the total value of stress in the middle layer to surpass the characteristic strength earlier than in the bottom layer. The crack therefore would initiate in the middle of the specimen and not on the bottom side.

5.5.2 2nd configuration of layers

The meaning of the word configuration in this sense means different thicknesses of the layers. Material properties remain the same. Only limited amount of different material properties were available and the ones chosen present values suitable for the demonstration of the effect residual stresses have. The dimensions of the model also remain the same since for the demonstration of this effect it is desired that the total volume does not change. The new thicknesses of the layers are listed in table (18).

Table 18: Thicknesses of the 2nd configuration of layers.

Layer thickness	Value
t_1	$0,25$ mm
t_2	$0,5$ mm
t_3	$0,25$ mm

The values of the CTEs are also unchanged. The same value of force (450 N) was used as it provides usable values of 1st principal stress in the evaluated locations as well. The change in configuration of the layer thicknesses changes the values of the residual stresses. Figure (36) shows current values of the stresses.

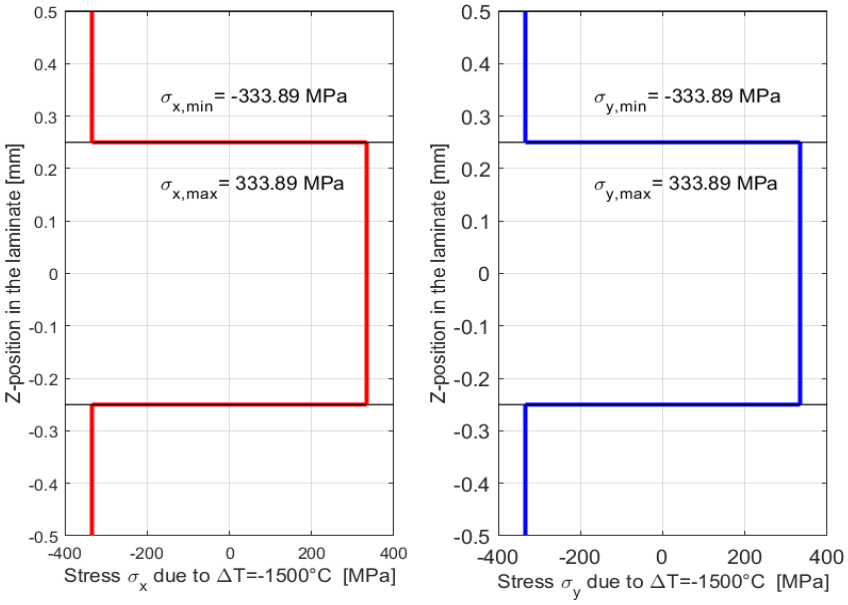

Figure 36: Values of residual stress over the thickness of the laminate in both directions (2nd configuration).

This configuration of the laminate assigns each material half of the total volume which results in equal values of the stresses in tension and compression. Resulting stress values are presented in table (19) the same way as in the previous configuration.

Table 19: Different stresses of the 2nd configuration of layers.

Location \ Stress [MPa]	σ_1	σ_{RES}	σ_0	Total
Bottom of 1st layer	763,39	-333,89	485	429,50
Bottom of 2nd layer	333,36	333,89	645	667,25

Also in this case without the residual stress the characteristic strength would be surpassed at the bottom of the specimen. But because the same concept applies, the residual stress allows the bottom layer to withhold otherwise critical mechanical load. And because the inner layer is subjected to additional tensile stress, failure would occur there.

5.5.3 3rd configuration of layers

The last configuration assigns the outer material the least volume. Table (20) lists values of thicknesses used in this configuration.

Table 20: Thicknesses of the 3rd configuration of layers.

Layer thickness	Value
t_1	$0,15$ mm
t_2	$0,7$ mm
t_3	$0,15$ mm

The same loading force of 450 N was used. Since the thickness distribution was changed again the residual stress values changed again. New values are shown the figure (37).

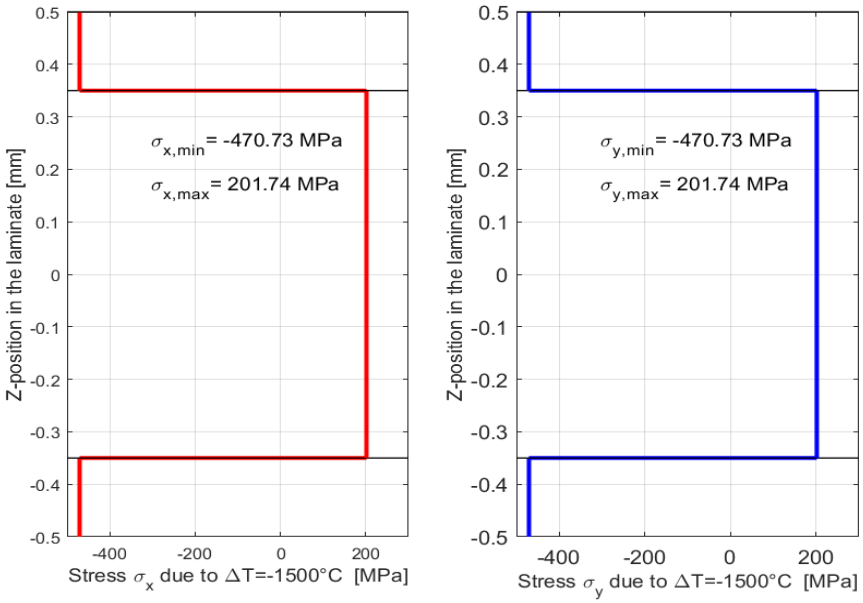

Figure 37: Values of residual stress over the thickness of the laminate in both directions (3rd configuration).

The evaluation of all the stress values is presented in table (21).

Table 21: Different stresses of the 3rd configuration of layers.

Location \ Stress	σ_1	σ_{RES}	Characteristic strength	Total
Bottom of 1st layer	774,91	-470,73	485	304,18
Bottom of 2nd layer	471,44	201,75	645	673,19

The same outcome can be seen for this configuration as well. With 3 calculations performed it is obvious that effect of residual stresses can effect not only the stress distribution of a specimen, but also cause fracture of a specimen in various places.

With increasing thickness of the inner layer higher negative values of residual stress can be observed. This means that if specimen does not break from increasing value of residual stress during cooling after sintering, it is more likely it breaks on one of the inner layers.

6 Conclusion

This thesis dealt with a modelling of the B3B test using models with various shapes and curvatures of specimens. Laminated specimens were also modelled. Both disc and plate shapes of the model were considered. Models were at first considered to be monolithic and flat. After that the effect of curvature was included. Lastly, the model was enhanced by the presence of multiple layers. In all previous models unitary load was applied. In the last part, the effect of residual stresses was included.

At first, models for flat specimen were created. For these models calculations were performed for various values of the models thickness. For both models in total 6 different values of thicknesses were considered ranging from $0,250$ to $2,0$ mm. From each calculation, values of the 1st principal stress at the bottom of the specimen was obtained as well as the f factor. Since unitary load was applied, the values of the stress obtained did not represent actual fracture stress. It was proven that if certain conditions are met, the value of f factor is not dependant on the applied loads. It was shown that both stress and the f factor depend on the thickness of both models with a hyperbolic trend. Data were fitted with a very good precision.

Next, the effect of specimen curvature was included into the model. Its effect was dependent on the distance between the centre of the specimen and its edge in the z direction, which is the same for all used models. This was interpreted through parameters $w_{d,p1,p2}$. One model was created to simulate a disc specimen. Two models describing curved plate specimens were created. First curved plate model included the effect of curvature in only one direction. Second plate model included the curvature for both sides. For each model six different values of curvature were calculated. This led to graphs showing the relation between f factor and curvature. All data tended towards linear relation between f factor values and curvature.

The effect of curvature was also shown on models that include multiple layers. All three curved models were layered. For each of them a variant with 3, 4 and 5 layers was created. For chosen configurations of curved model/number of layers the same calculations were preformed. Even in these cases the relation between f factor and curvature seemed linear. This was also then shown via parameters describing the goodness of a fit.

On a model of a laminated disc it was shown that it is possible for the specimen

to break at the interface of layers rather than at the bottom of the first layer. This effect is more likely to occur if the material properties of the neighbouring layers have high differences in their values.

In the last part of the thesis the effect of residual stresses was included in the layered model. A model of the flat plate with 3 layers was used. The thicknesses of layers were chosen such that the laminate was symmetrical which resulted in a constant residual stress throughout the thickness of each layer. On three different configurations of layers thicknesses it was shown that residual stress may result in fracture of the specimen in locations other than the bottom surface. Used values of the CTE were relatively close to each other because of the materials considered for the demonstration of the effect. For different set of materials with higher mismatch in CTE values, effect of shielding by compressive residual stress and weakening by tensile residual stress could play even stronger role.

References

[1] Tanja Lube, Walter Harrer and Peter Supancic. *Practical Guide to Ball-on-Three-Balls (B3B) Testing*. Tech. rep. Leoben: Institut für Struktur- und Funktionskeramik, Montanuniversität Leoben, Jan. 2017. 7 pp.

[2] Přemysl Janíček. *Systémová metodologie. brána do řešení problémů*. Brno: Akademické nakladatelství CERM, 2014. ISBN: 978-80-7204-887-8.

[3] *Techická keramika*. 2021. URL: `http://ime.fme.vutbr.cz/images/umvi/vyuka/struktura_a_vlastnosti_materialu/prednasky/12%5C%20-%5C%20Keramika.pdf` (visited on 21/05/2021).

[4] *Keramické materiály*. 2021. URL: `http://ime.fme.vutbr.cz/images/umvi/vyuka/bum/prednasky/10-BUM%5C%20-%5C%20keramicke%5C%20materialy.pdf` (visited on 21/05/2021).

[5] Mrázková L. "Napěťová analýza zatěžovaného disku pro zkoušku pevnosti v ohybu." Diplomová práce. Brno: Vysoké učení technické v Brně, Fakulka strojního inženýrství, 2006.

[6] Přemysl Janíček. *Mechanika těles. pružnost a pevnost I*. Brno: Akademické nakladatelství CERM, 2004. ISBN: 80-214-2592-X.

[7] W. D. Kingery, H. K. Bowen and D. R. Uhlmann. *Introduction to ceramics*. 2nd ed. New York: Wiley, 1976. ISBN: 04-714-7860-1.

[8] Jaroslav Juračka. *Kompozitní konstrukce v letectví*. 10. Brno: Letecký ústav, VUT v Brně, 207.

[9] Andreas Börger, Peter Supancic and Robert Danzer. "The ball on three balls test for strength testing of brittle discs. stress distribution in the disc". In: *Journal of the European Ceramic Society* 22.9-10 (2002), pp. 1425–1436. ISSN: 09552219. DOI: 10.1016/S0955-2219(01)00458-7. URL: `https://linkinghub.elsevier.com/retrieve/pii/S0955221901004587` (visited on 18/05/2021).

[10] *Fine ceramics (advanced ceramics, advanced technical ceramics) — Mechanical properties of monolithic ceramics at room temperature — Determination of flexural strength by the ring-on-ring test*. 1. Leoben: ISO, 2018.

[11] *Standard Test Method for Monotonic Equibiaxial Flexural Strength of Advances Ceramics at Ambient Temperature*. 5. West Conshohocken, PA, USA, 2005.

[12] C. Barry Carter and M. Grant Norton. *Ceramic materials. science and engineering*. New York: Springer, 2007. ISBN: 03-874-6270-8.

[13] J. Kovář. "Pravděpodobnosti porušení keramické součásti s využitím Weibullovy teorie nejslabšího článku". Diplomová práce. Vysoké učení technické v Brně, Fakulka strojního inženýrství, 2018.

[14] L. Afferrante, M. Ciavarella and E. Valenza. "Is Weibull's modulus really a material constant? Example case with interacting collinear cracks". In: *International Journal of Solids and Structures* 43.17 (2006), pp. 5147–5157. ISSN: 00207683. DOI: 10.1016/j.ijsolstr.2005.08.002. URL: https://linkinghub.elsevier.com/retrieve/pii/S0020768305005226 (visited on 21/05/2021).

[15] Stefan Strobl et al. "Fracture toughness testing of small ceramic discs and plates". In: *Journal of the European Ceramic Society* 36.6 (June 2014), pp. 1637–1642. ISSN: 0955-2219. DOI: 10.1016/j.jeurceramsoc.2013.12.021. URL: https://www.sciencedirect.com/science/article/pii/S0955221913005943.

[16] Andreas Börger, Peter Supancic and Robert Danzer. "The ball on three balls test for strength testing of brittle discs. Part II: analysis of possible errors in the strength determination". In: *Journal of the European Ceramic Society* 24.10-11 (Sept. 2004), pp. 2917–2928. ISSN: 0955-2219. DOI: 10.1016/j.jeurceramsoc.2003.10.035. URL: https://www.sciencedirect.com/science/article/pii/S0955221903008458.

[17] Robert Danzer et al. "The ball on three balls test. Strength and failure analysis of different materials". In: *Journal of the European Ceramic Society* 27.2-3 (Sept. 2007), pp. 1481–1485. ISSN: 0955-2219. DOI: 10.1016/j.jeurceramsoc.2006.05.034. URL: https://www.sciencedirect.com/science/article/pii/S0955221906003669.

[18] Xinyuan Mao and Hideaki Takahashi. "Development of a further-miniaturized specimen of 3 mm diameter for tem disk (ø 3 mm) small punch tests". In: *Journal of Nuclear Materials* 150.1 (1987), pp. 42–52. ISSN: 00223115. DOI:

10.1016/0022-3115(87)90092-4. URL: https://linkinghub.elsevier.com/retrieve/pii/0022311587900924 (visited on 21/05/2021).

[19] Tanja Lube, Stefan Rasche and Tjokorda Gde Tirta Nindhia. "A Fracture Toughness Test Using the Ball-on-Three-Balls Test". In: *Journal of the European Ceramic Society* 36.6 (Oct. 2015), pp. 1637–1642. ISSN: 1551-2916. DOI: 10.1111/jace.13842. URL: https://ceramics.onlinelibrary.wiley.com/doi/full/10.1111/jace.13842.

[20] *Circular segment*. 1987. URL: https://mathworld.wolfram.com/CircularSegment.html (visited on 21/05/2021).

[21] Zdeněk Chlup et al. "Effect of residual stresses to the crack path in alumina/zirconia laminates". In: *Journal of the European Ceramic Society* 40.15 (2020), pp. 5810–5818. ISSN: 09552219. DOI: 10.1016/j.jeurceramsoc.2020.06.044. URL: https://linkinghub.elsevier.com/retrieve/pii/S0955221920305148 (visited on 21/05/2021).

[22] Josef Schlacher et al. "Additive manufacturing of high-strength alumina through a multi-material approach". In: *Open Ceramics* 5 (2021). ISSN: 26665395. DOI: 10.1016/j.oceram.2021.100082. URL: https://linkinghub.elsevier.com/retrieve/pii/S2666539521000286 (visited on 21/05/2021).

List of symbols

a	[mm]	Edge length of a plate specimen for the B3B test
a_{4P}	[mm]	Distance from support to the load in 4 point bending test
a_{KI}	[mm]	Depth of a crack in tests for evaluating the fracture toughness
b	[mm]	Width of a specimen for bending tests
d	[mm]	Diameter of a specimen for bending tests
E	[MPa]	Young's modulus
f	[-]	f factor
F	[N]	Applied force
F_{max}	[N]	Maximal force
h	[mm]	Height of a specimen for bending tests
K_{Ic}	[MPa$\sqrt{\text{m}}$]	Fracture toughness
l	[mm]	Length of a specimen for bending tests
m	[-]	Weibull modulus
n	[-]	Number of layers of a laminate
R,r	[mm]	Radius of the specimen in the B3B test
R_a,r_a	[mm]	Support radius in the B3B test
R_b,r_b	[mm]	Ball radius in the B3B test
S	[mm^2]	Area of cross section
t	[mm]	Thickness of a specimen in the B3B test
$w_{d,p1,p2}$	[mm]	Distance from the center of the specimen to its edge (disc and both plates)
Y	[-]	Geometry factor of tests for evaluating the fracture toughness
z_{diff}	[mm]	Lowest distance from specimen to its center of curvature
α	[K^{-1}]	Coefficient of thermal expansion
ε	[-]	Strain
κ	[mm^{-1}]	Curvature
ν	[-]	Poisson's ratio
ρ	[mm]	Radius of curvature
σ_0	[MPa]	Characteristic strength
$\sigma_{I,II,II}$	[MPa]	Principal stresses (not ordered)
$\sigma_{1,2,3}$	[MPa]	Principal stresses (ordered)

$\sigma_{eq,PIA}$	[MPa]	PIA equivalent stress
σ_{max}	[MPa]	Maximal stress
σ_{Rd}	[MPa]	Compression strength
σ_{RES}	[MPa]	Residual stress
σ_{UTS}	[MPa]	Ultimate tensile strength
σ_y	[MPa]	Yields stress
φ	[°]	Angle of offset

List of Figures

List of Tables